iScience

CellPress
OPEN ACCESS

Article

Preclinical validation of human recombinant glutamate-oxaloacetate transaminase for the treatment of acute ischemic stroke

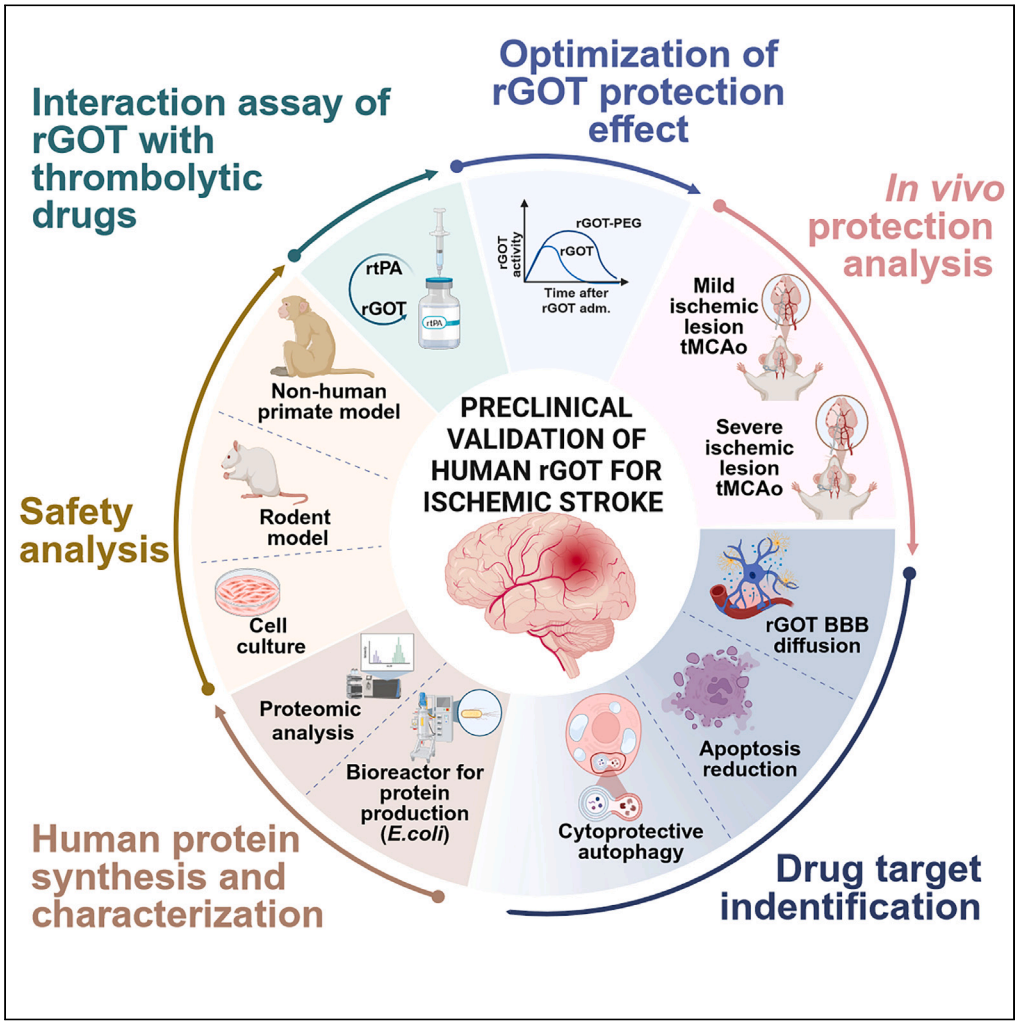

María Pérez-Mato, Antonio Dopico-López, Yunus Akkoc, ..., David Mirelman, José Castillo, Francisco Campos

francisco.campos.perez@sergas.es

Highlights

rGOT mediates protection after stroke by crossing the blood-brain barrier

rGOT reduces neuronal apoptosis and induces cytoprotective autophagy

A sustained increase in GOT activity for at least 8 h was needed to achieve protection

rGOT can be safely combined with thrombolytic therapies

Pérez-Mato et al., iScience 27, 111108
November 15, 2024 © 2024 The Author(s). Published by Elsevier Inc.
https://doi.org/10.1016/j.isci.2024.111108

iScience

CellPress
OPEN ACCESS

Article

Preclinical validation of human recombinant glutamate-oxaloacetate transaminase for the treatment of acute ischemic stroke

María Pérez-Mato,[1,2,24] Antonio Dopico-López,[1,24] Yunus Akkoc,[3,18] Sonia López-Amoedo,[1] Clara Correa-Paz,[1] María Candamo-Lourido,[1] Ramón Iglesias-Rey,[4] Esteban López-Arias,[1] Ana Bugallo-Casal,[1] Andrés da Silva-Candal,[5] Susana B. Bravo,[6] María del Pilar Chantada-Vázquez,[6,7] Susana Arias,[8] María Santamaría-Cadavid,[8] Ana Estany-Gestal,[9] Ahlem Zaghmi,[10,11] Marc A. Gauthier,[10] María Gutiérrez-Fernández,[2] Abraham Martin,[12,13] Jordi Llop,[14] Cristina Rodríguez,[15,16] Ángeles Almeida,[15,16] Martina Migliavacca,[17] Ester Polo,[17] Beatriz Pelaz,[17] Devrim Gozuacik,[3,18] Naouale El Yamani,[19] Tanima SenGupta,[19] Elise Rundén-Pran,[19] José Vivancos,[20] Mar Castellanos,[5] Exuperio Díez-Tejedor,[2] Tomás Sobrino,[21,22] Aharon Rabinkov,[23] David Mirelman,[23] José Castillo,[4] and Francisco Campos[1,25,*]

SUMMARY

The blood enzyme glutamate-oxaloacetate transaminase (GOT) has been postulated as an effective therapeutic to protect the brain during stroke. To demonstrate its potential clinical utility, a new human recombinant form of GOT (rGOT) was produced for medical use.

We tested the pharmacokinetics and evaluated the protective efficacy of rGOT in rodent and non-human primate models that reflected clinical stroke conditions.

We found that continuous intravenous administration of rGOT within the first 8 h after ischemic onset significantly reduced the infarct size in both severe (30%) and mild lesions (48%). Cerebrospinal fluid and proteomics analysis, in combination with positron emission tomography imaging, indicated that rGOT can reach the brain and induce cytoprotective autophagy and induce local protection by alleviating neuronal apoptosis.

Our results suggest that rGOT can be safely used immediately in patients suspected of having a stroke. This study requires further validation in clinical stroke populations.

[1]Translational Stroke Laboratory Group (TREAT), Clinical Neurosciences Research Laboratory (LINC), Health Research Institute of Santiago de Compostela (IDIS), 15706 Santiago de Compostela, Spain
[2]Neurological Sciences and Cerebrovascular Research Laboratory, Department of Neurology, Neurology and Cerebrovascular Disease Group, Neuroscience Area of Hospital La Paz Institute for Health Research – IdiPAZ (La Paz University Hospital- Universidad Autónoma de Madrid), 28029 Madrid, Spain
[3]Koç University Research Center for Translational Medicine (KUTTAM), Istanbul 34450, Turkey
[4]Neuroimaging and Biotechnology Laboratory Group (NOBEL), Clinical Neurosciences Research Laboratory (LINC), Health Research Institute of Santiago de Compostela (IDIS), 15706 Santiago de Compostela, Spain
[5]Neurology Service, University Hospital Complex of A Coruña, A Coruña Biomedical Research Institute, 15006 A Coruña, Spain
[6]Proteomic Unit, Health Research Institute of Santiago de Compostela (IDIS), 15706 Santiago de Compostela, Spain
[7]Research Unit, Lucus Augusti University Hospital (HULA), Servizo Galego de Saúde (SERGAS), 27002 Lugo, Spain
[8]Stroke Unit, Department of Neurology, Hospital Clínico Universitario, 15706 Santiago de Compostela, Spain
[9]Unit of Methodology of the Research, Health Research Institute of Santiago de Compostela (IDIS), 15706 Santiago de Compostela, Spain
[10]Institut National de la Recherche Scientifique (INRS), EMT Research Center, Varennes, QC J3X 1S2, Canada
[11]Rheumatology Unit, Department of Medicine, Karolinska Institutet, Karolinska University Hospital, 171 77 Stockholm, Sweden
[12]Achucarro Basque Center for Neuroscience, 48940 Leioa, Spain
[13]Ikerbasque Basque Foundation for Science, 48009 Bilbao, Spain
[14]CIC biomaGUNE, Basque Research and Technology Alliance (BRTA), 20014 San Sebastian, Spain
[15]Institute of Functional Biology and Genomics (IBFG), CSIC, University of Salamanca, 37007 Salamanca, Spain
[16]Institute of Biomedical Research of Salamanca (IBSAL), University Hospital of Salamanca, CSIC, University of Salamanca, 37007 Salamanca, Spain
[17]Center for Research in Biological Chemistry and Molecular Materials (CiQUS), University of Santiago de Compostela, 15705 Santiago de Compostela, Spain
[18]Department of Medical Biology, Koç University School of Medicine, Istanbul 34450, Turkey
[19]Health Effects Laboratory, Department for Environmental Chemistry, NILU-Norwegian Institute for Air Research, 2027 Kjeller, Norway
[20]Stroke Unit, Department of Neurology, Hospital Universitario de La Princesa & Instituto de Investigación Sanitaria La Princesa, 28006 Madrid, Spain
[21]NeuroAging Group (NEURAL), Clinical Neurosciences Research Laboratory (LINC), Health Research Institute of Santiago de Compostela (IDIS), 15706 Santiago de Compostela, Spain
[22]Centro de Investigación Biomédica en Red en Enfermedades Neurodegenerativas (CIBERNED), Instituto de Salud Carlos III, 28029 Madrid, Spain
[23]Department of Biomolecular Sciences, Weizmann Institute of Science, Rehovot 7610001, Israel
[24]These authors contributed equally
[25]Lead contact
*Correspondence: francisco.campos.perez@sergas.es
https://doi.org/10.1016/j.isci.2024.111108

This is an open access article under the CC BY-NC-ND license (http://creativecommons.org/licenses/by-nc-nd/4.0/).

INTRODUCTION

Glutamate-oxaloacetate transaminase (GOT), also known as aspartate transaminase, is a pyridoxal phosphate-dependent transaminase enzyme that exists in cytoplasmic and inner-membrane mitochondrial forms, known as GOT1 and GOT2, respectively. Both forms catalyze the reversible transamination of oxaloacetate and glutamate to aspartate and α-ketoglutarate and play an essential role in amino acid metabolism in the urea and tricarboxylic acid cycles[1,2] (critical pathways of cell energy homeostasis), as well as in other metabolic programs.[3]

In clinical settings, blood GOT levels are used as indicators of liver and muscle damage or myocardial infarction.[4] However, based on its ability to modulate glutamate metabolism, exogenous administration of the recombinant form of GOT1 (rGOT) has been proposed as a therapy to reduce neuronal damage in pathologies such as traumatic brain injury,[5] post-stroke depression,[6] glioma,[7] Alzheimer's disease,[8] amyotrophic lateral sclerosis,[9] and acute stroke.[10–13]

In the field of stroke pathology, the therapeutic mechanisms postulated to be responsible for the protective effect of rGOT are mainly associated with the metabolism and reduction of blood glutamate, which results in a lower increase in pathological glutamate caused by stroke in the cerebral parenchyma.[10] Other studies have also reported that GOT metabolizes brain glutamate as an energy substrate in anaerobic conditions such as ischemia.[7,11] This hypothesis is substantiated by the fact that the overexpression of GOT in the brain reduces the increase of glutamate and prevents the loss of ATP in ischemic conditions.[14,15] A recent study has also reported that mitochondrial GOT protects against energy failure after ischemia.[16]

The protective effect of rGOT against stroke has been mainly investigated through rodent ischemic models where intravenous rGOT administration has been associated with a reduction in ischemic lesions and better recovery.[17] Moreover, in the same animal models, inhibition of endogenous blood GOT activity prior to the induction of ischemic stroke resulted in more significant damage.[18] In two retrospective studies[19,20] of patients with stroke, high blood GOT activity levels were associated with good outcomes at 3 months, which suggests that exogenous administration of rGOT may be a potential stroke therapy.

To demonstrate the clinical value of GOT as a novel neuroprotective therapy for stroke, a new human form of rGOT for medical use was manufactured, and its tolerability and pharmacokinetics were tested in rat and non-human primate (NHP) models. We aimed to investigate the protective efficacy of rGOT using different experimental approaches that reflect clinical acute stroke conditions following arterial recanalization. Finally, we investigated the underlying mechanisms to clarify the observed protective response.

RESULTS

Pharmacokinetics and toxicity analysis of rGOT in rats and NHPs

To analyze the pharmacokinetics of this new human version of rGOT, increasing doses (0.06, 0.12, 0.24, 0.5, 1, 2, and 4 mg/kg) were administered intravenously (i.v.) to healthy rats. Blood samples were collected pre-dose (basal), hourly up to 6 h, and 10 days post-dose. Basal whole-blood GOT activity levels in rodents were determined to be 60–90 U/L, which is higher than that reported in humans (~40 U/L).[4] The mean whole blood GOT activity levels 1 h after treatment administration were 270 ± 40; 630 ± 100; 1,400 ± 90; 3,600 ± 900; 6,800 ± 400; 16,700 ± 2,200; and 30,000 ± 2,250 U/L, representing ~4-fold, 9-fold, 20-fold, 50-fold, 100-fold, 230-fold, and 400-fold increases, respectively (Figure 1A), with respect to basal levels. The activity levels returned to basal levels 24 h after administration. The mean half-life ($T_{1/2}$) of blood GOT activity following rGOT administration was ~2 h (Figure 1B). The tested doses did not have adverse effects on body weight, food consumption, or death in rodents.

Increasing doses of rGOT (0.12, 0.5, and 1 mg/kg) were later tested individually in the three NHPs. The average basal GOT level was 20–40 U/L, which is similar to that expected for healthy adults. The increase in blood GOT activity at 1 h was 101; 2,600; and 6,600 U/L, representing 5-fold, 100-fold, and 260-fold increases, respectively, relative to basal levels (Figure 1C). Pharmacokinetic analysis following a single dose of 1 mg/kg rGOT in a new group of four NHPs revealed a longer clearance time in NHPs than that in rats ($T_{1/2}$: 5 vs. 2 h) (Figure 1D). For safety and toxicity analyses, the same group of four NHPs treated with 1 mg/kg rGOT received a second dose of 5 mg/kg on day 14 after the first dose. Hematological (Table S1), biochemical (Table S2), and hemostatic (Table S3) parameters were evaluated on days 0, 1, 7, 14, 15, 21, and 42, as indicated in Figure S1A. Urine analysis (Table S4) was performed on days 0, 7, 14, and 21.

Treatment with rGOT was well tolerated by all the animals. No clinical signs or unexpected symptoms were observed at the injection sites following rGOT administration to the NHPs. No changes in food consumption or adverse variations in body weight were observed during the study. Hematology, biochemistry, coagulation, and urinalysis parameters did not show any significant variations and revealed no adverse effects of rGOT (Tables S5–S10). Immunogenicity analysis on days 0, 14, and 42 did not reveal the development of antibodies against rGOT in any of the NHP blood samples (Figure S1B). Only blood GOT activity levels showed significant variation in line with treatment response. Manufacturing and characterization of rGOT are presented in the supplemental information and Figures S2A–S2C.

Neuroprotective dose-response analysis for rGOT in *in vivo* models of ischemia

A previous study from our group established that a single dose of 0.12 mg/kg rGOT resulted in blood GOT levels of ~1,500 U/L (21-fold increase with respect to basal levels) and neuroprotection in ischemic animal models.[17] Based on these previous findings, the new human form of rGOT was tested in the same ischemic model using 75 min of transient intra-filament occlusion of the middle cerebral artery (tMCAO), starting with a dose of 0.24 mg/kg required to achieve a blood GOT activity level close to 1,500 U/L (1,400 ± 90 U/L). Treatment was administered as a single i.v. bolus at different time points in independent groups of ischemic animals (i.e., either immediately after artery reperfusion

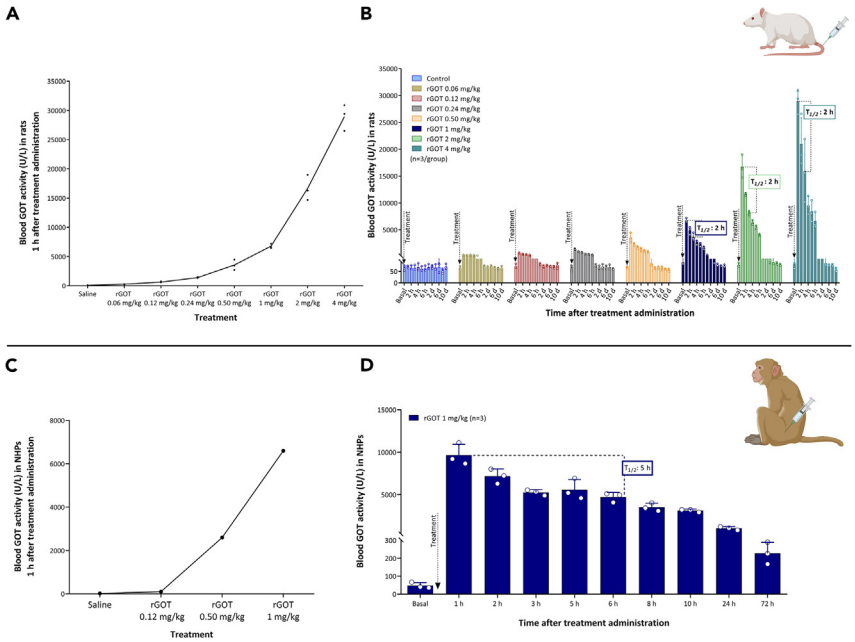

Figure 1. Pharmacokinetic analysis of rGOT in rats and primates

(A) Dose-response curve of blood GOT activity measured 1 h after rGOT i.v. administration in healthy rats (*n = 3*).

(B) Time course of blood GOT activity in healthy rats treated with rGOT. Rats were i.v. treated with saline (control group) and rGOT (0.06, 0.12, 0.24, 0.5, 1, 2, and 4 mg/kg). Blood GOT activity was measured under basal conditions (before treatment administration) and 1, 2, 3, 4, 5, and 6 h and 1, 2, 4, 6, 8, and 10 days after administration. The dashed line represents the half-life ($T_{1/2}$ = 2 h) of rGOT.

(C) Dose-response analysis in healthy primates (*n* = 1/dose) treated with 0.12, 0.5, and 1 mg/kg rGOT. Blood GOT activity before treatment was considered the basal value. GOT blood activity was determined 1 h after treatment administration.

(D) Pharmacokinetic analysis of a 1 mg/kg dose in healthy primates (*n = 3*). Blood GOT activity was measured under basal conditions (before treatment administration) and 1, 2, 3, 5, 6, 8, and 10 h, and 1 and 3 days after administration. The $T_{1/2}$ of rGOT was estimated to be around 5 h. Data are shown as mean ± standard deviation of the mean. The data were analyzed using SPSS statistical software (v19.0) and GraphPad Prism software (v.8.3.0) for representation of graphs. i.v., intravenous; NHPs, non-human primates; rGOT, recombinant glutamate-oxaloacetate transaminase. BioRender (https://biorender.com/) was used for creating the figures.

[75 min post-cerebral occlusion] or 1, 2, 4, and 6 h after reperfusion; see schematic representation in Figure S3A). In all rGOT-treated groups, the blood GOT activity increased to ~1,500 U/L from the basal value of 70 U/L (Figure S3B). To evaluate the protective efficacy of rGOT, the size of the ischemic lesion was measured by MRI on day 0 (during cerebral artery occlusion) and on days 1, 7, and 14 after ischemia induction. Basal lesion assessment at day 0 and before treatment administration confirmed similar lesion volumes in all the included animals (35%–45%, established as the percentage of ischemic damage with respect to the ipsilateral hemisphere volume, corrected for brain edema, Figures S3C and S3D). At this dose of rGOT, no effect on infarct volume was observed in any of the treated groups.

This lack of effectiveness led to a dose-escalation study (0.24, 0.5, 1, 2, and 4 mg/kg rGOT) with rGOT administered in all cases immediately after arterial reperfusion (75 min after tMCAO) (Figure 2A). All treatments caused a significant dose-response increase in blood GOT activity with respect to the basal levels (70 ± 10 U/L), with peak activities at 1 h: 1,300 ± 100; 2,700 ± 600; 6,000 ± 2,000; 10,000 ± 3,000; and 23,000 ± 4,000 U/L (Figure 2B) in order of increasing dose. Assessment of infarct volume (Figures 2C and 2D) showed no significant reduction in infarct size in treated animals at any of the doses tested. Only the 1 mg/kg dose (which resulted in a ~100-fold increase in blood GOT levels) induced a significant functional improvement compared to the control group at day 7 (Figure 2E).

Oxaloacetate acid (OAA) is a critical co-substrate for the transamination of glutamate to aspartate and α-ketoglutarate by GOT.[17] To evaluate whether this co-substrate could act as a limiting factor in the activity of rGOT, a dose of 1 mg/kg rGOT was supplemented with OAA at three increasing doses of 0.35, 3.5, and 35 mg/kg. The results (Figures S4A–S4C) show that OAA did not enhance the effect of 1 mg/kg rGOT in terms of blood GOT activity or brain protection.

To maintain a sustained increase in GOT activity within the first hours after the ischemia onset, a new study was initiated based on multiple injections of rGOT. Different administration protocols were evaluated in healthy rats (Figures S5A–S5C). The selected protocol, validated in rodent ischemic conditions and healthy NHP models (Figures S5D and S5E), consisted of four doses of rGOT over an 8 h period, with an interval of 2–3 h between doses.

The therapeutic effect of the selected protocol was evaluated using the dose range tested previously, starting at 0.24, 0.5, 1, 2, and 4 mg/kg, as shown in Figure 2F. All rGOT treatments induced an increase in blood GOT activity, which was maintained for up to 24 h after the first administration (Figure 2G). The values of blood GOT activity at 8 h were 2,100 ± 700; 4,000 ± 2,000; 8,000 ± 2,000; 17,000 ± 3,000;

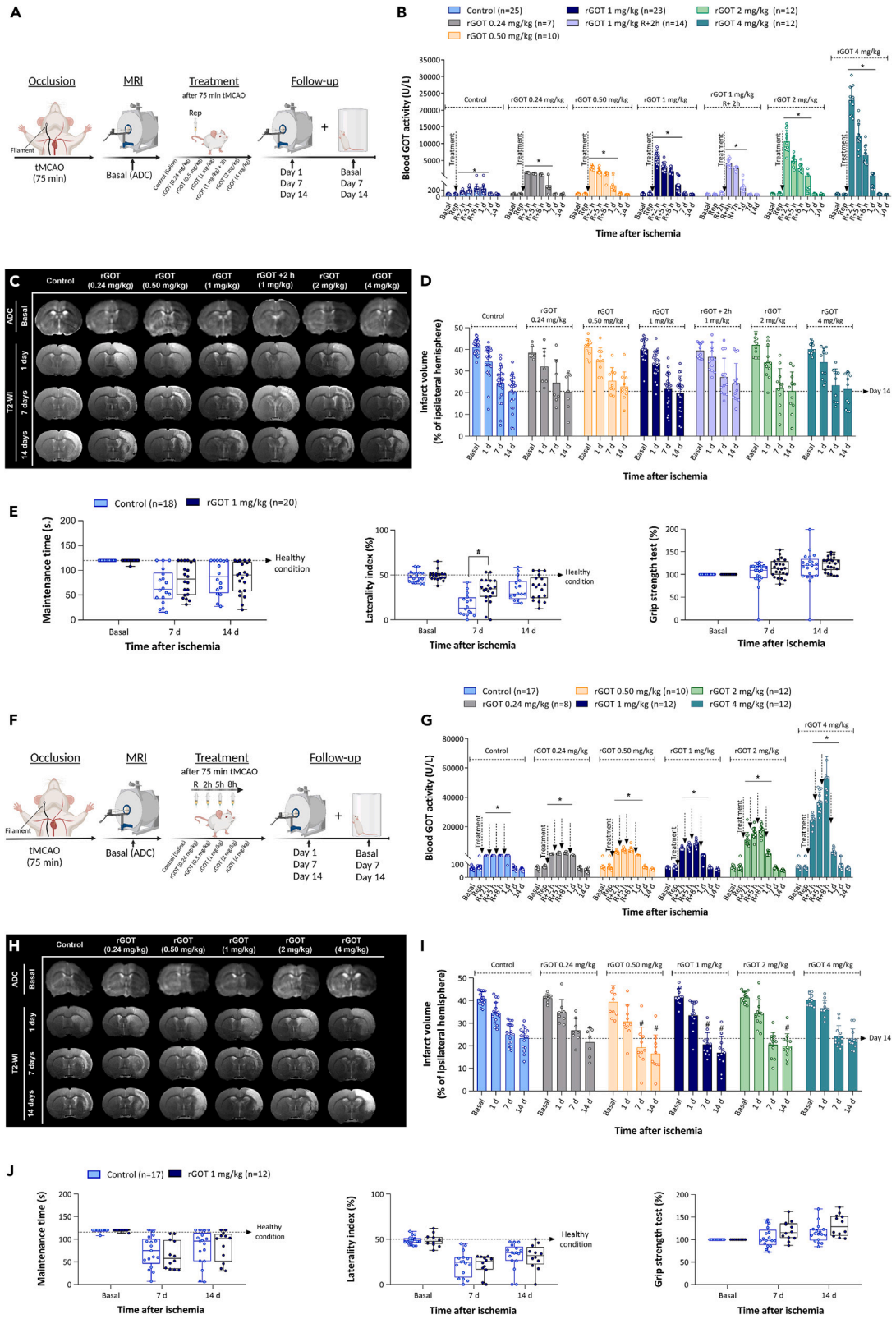
A
Occlusion
MRI
Treatment
after 75 min tMCAO
Follow-up
Filament
tMCAO
(75 min)
Basal (ADC)
Rep
Day 1
Day 7
Day 14
Basal
Day 7
Day 14
B
Control (n=25)
rGOT 0.24 mg/kg (n=7)
rGOT 0.50 mg/kg (n=10)
rGOT 1 mg/kg (n=23)
rGOT 1 mg/kg R+2h (n=14)
rGOT 2 mg/kg (n=12)
rGOT 4 mg/kg (n=12)
Blood GOT activity (U/L)
Time after ischemia
C
Control
rGOT (0.24 mg/kg)
rGOT (0.50 mg/kg)
rGOT (1 mg/kg)
rGOT +2 h (1 mg/kg)
rGOT (2 mg/kg)
rGOT (4 mg/kg)
ADC
Basal
T2-WI
1 day
7 days
14 days
D
Infarct volume (% of ipsilateral hemisphere)
Day 14
Time after ischemia
E
Control (n=18)
rGOT 1 mg/kg (n=20)
Maintenance time (s)
Healthy condition
Laterality index (%)
Grip strength test (%)
Time after ischemia
F
Occlusion
MRI
Treatment
after 75 min tMCAO
R 2h 5h 8h
Follow-up
Filament
tMCAO
(75 min)
Basal (ADC)
Day 1
Day 7
Day 14
Basal
Day 7
Day 14
G
Control (n=17)
rGOT 0.24 mg/kg (n=8)
rGOT 0.50 mg/kg (n=10)
rGOT 1 mg/kg (n=12)
rGOT 2 mg/kg (n=12)
rGOT 4 mg/kg (n=12)
Blood GOT activity (U/L)
Time after ischemia
H
Control
rGOT (0.24 mg/kg)
rGOT (0.50 mg/kg)
rGOT (1 mg/kg)
rGOT (2 mg/kg)
rGOT (4 mg/kg)
ADC
Basal
T2-WI
1 day
7 days
14 days
I
Infarct volume (% of ipsilateral hemisphere)
Day 14
Time after ischemia
J
Control (n=17)
rGOT 1 mg/kg (n=12)
Maintenance time (s)
Healthy condition
Laterality index (%)
Grip strength test (%)
Time after ischemia

Figure 2. Therapeutic study of rGOT in rats with severe cerebral ischemia

(A) Schematic representation of the experimental design. Treatments (saline and rGOT at 0.24, 0.5, 1, 2, and 4 mg/kg) were administered as a single i.v. bolus immediately after artery reperfusion (75 min after cerebral occlusion) in independent groups of ischemic animals. Dose of 1 mg/kg administered 2 h after reperfusion was tested in an additional experimental group. Ischemic lesion was measured by MRI at day 0 by ADC maps (during cerebral artery occlusion), and at days 1, 7, and 14 after ischemia induction by T2-maps. Basal lesion assessment at day 0 was used to confirm similar lesion volumes (35%–45%) in all included animals before treatment administration. Motor and somatosensory tests were evaluated by means of rotarod test, grip strength, and cylinder test at 1 day before surgery (basal) and 7 and 14 days after ischemia.

(B) Time course of blood GOT activity in ischemic rats.

(C) MRI analysis of the ischemic evolution.

(D) Infarct size assessment in ischemic rats. Ischemic lesion is represented as percentage adjusted to the ipsilateral hemisphere. The dashed line represents the infarct volume at 14 days of the control group used as reference to see the effect of treatments.

(E) Boxplots showing the assessment of sensorimotor function using rotarod test (evaluated as maintenance time in seconds), cylinder test (evaluated as percentage of laterality), and grip strength (evaluated as percentage with respect to the basal condition). The dashed line in the rotarod and cylinder tests represents the healthy condition of the animals before the ischemic induction. In the grip strength, natural increase of muscular strength is reduced by ischemic lesion.

(F) Schematic representation of the experimental design. Treatments (saline and rGOT, 0.24, 0.5, 1, 2, and 4 mg/kg) were administered (i.v.) in independent groups of ischemic animals four times over a period of 8 h. The first dose was initiated after artery reperfusion (75 min after cerebral occlusion), followed by three consecutive doses at 2, 5, and 8 h after artery reperfusion. The ischemic lesion was measured by MRI at day 0 by ADC maps (during cerebral artery occlusion), and at days 1, 7, and 14 after ischemia induction by T2-maps. Basal lesion assessment at day 0 was used to confirm similar lesion volumes (35%–45%) in all included animals before treatment administration. Motor and somatosensory tests were evaluated by means of the rotarod test, grip strength test, and cylinder test at 1 day before surgery (basal), and 7 and 14 days after ischemia.

(G) Time course of blood GOT activity in ischemic rats.

(H) MRI analysis of the ischemic evolution.

(I) Infarct size assessment in ischemic rats.

(J) Boxplots showing the assessment of sensorimotor function using the rotarod test (evaluated as maintenance time in seconds), cylinder test (evaluated as percentage of laterality), and grip strength (evaluated as percentage with respect to the basal condition). The dashed line in the rotarod and cylinder tests represents the healthy condition of the animals before the ischemic induction. In the grip strength, natural increase of muscular strength is reduced by ischemic lesion. All data are expressed as mean ± standard deviation of the mean. p * < 0.05 compared with the basal. p # < 0.05 compared with the control group at same time point. The data were analyzed using SPSS statistical software (v19.0) and GraphPad Prism software (v.8.3.0) for representation of graphs. The criterion for statistical significance was set at $p < 0.05$. The Shapiro–Wilk test was used to determine whether the data were normally distributed. Based on the results of normality tests and the sample size, statistical analysis was performed using non-parametric tests, Wilcoxon test for paired data, and Mann-Whitney test for unpaired data. ADC, apparent diffusion coefficient; i.v., intravenous; MRI, magnetic resonance imaging; R or Rep, reperfusion; tMCAO, transient middle cerebral artery occlusion; rGOT, recombinant glutamate-oxaloacetate transaminase; T2-WI, T2-weighted imaging. BioRender (https://biorender.com/) was used for creating the figures.

and 50,000 ± 10,000 U/L (in order of increasing dose). Assessment of the ischemic lesion showed a significant protective effect with doses ranging from 0.5 to 2 mg/kg relative to the control group at day 14 (control group, infarct volume: 23% ± 2% vs. 0.5 mg/kg dose, 16% ± 5%; 1 mg/kg dose, 17% ± 3%; 2 mg/kg dose, 20% ± 5%; $p < 0.05$, Figures 2H and 2I). For these three doses, the data indicate an approximate 20%–30% reduction in ischemic lesions. Infarct protection was correlated with functional motor recovery in the rotarod and grip tests at 14 days in the 1 mg/kg rGOT group only compared to the control group, although the p values did not reach a significant level ($p = 0.048$ and $p = 0.046$) (Figure 2J).

Protective effect of rGOT in ischemic rats with mild lesions

To investigate if the reperfusion time could determine the efficacy of the therapy, the most effective doses obtained from the previous analysis (0.5 and 1 mg/kg) were tested in a mild ischemic animal model that was subjected to 45 min of tMCAO (Figure 3). Forty-five minutes of cerebral occlusion caused an average infarct size of 24% ± 4% at 24 h, which was significantly smaller than that achieved after 75 min of severe ischemia (34% ± 4%). A single 1 mg/kg dose of rGOT did not improve the protective efficacy against mild lesions (Figures 3A–3D). On the other hand, four consecutive administrations of 0.5 or 1 mg/kg rGOT led to significant infarct reduction, mainly at 14 days (lesion size on day 14, control: 11% ± 3% vs. 0.5 mg/kg dose, 9% ± 4%; 1 mg/kg dose: 6% ± 3%, $p < 0.05$, compared with the control; Figures 3E–3I). These data reflect a lesion reduction of ~20% with a dose of 0.5 mg/kg and 48% with a dose of 1 mg/kg on day 14 under mild ischemic conditions. Infarct reduction was correlated with functional motor recovery in the rotarod test (Figure 3J). The benefit of protection was lost when the 1 mg/kg dose was delayed to 2 h after reperfusion.

Bioconjugation of rGOT to extend the circulatory half-life

The aforementioned dose-response analyses with one and four consecutive administrations suggest that the protective effect of rGOT is mainly time dependent rather than dose dependent. Indeed, the protective benefit of rGOT disappeared at doses >2 mg/kg.

In a recent study, a bioconjugate form of rGOT modified with polyethylene glycol (rGOT-PEG) was able to maintain high levels of GOT activity (between 3,000 and 6,000 U/L) over a period of ~6 days following a single administration.[21] To investigate the hypothesis that the protective effects of rGOT are time dependent, a new experiment was designed to compare the administration of one and four doses of 1 mg/kg rGOT with one dose of 1 mg/kg rGOT-PEG, administered 75 min after cerebral occlusion in the same ischemic rat model (Figure 4A).

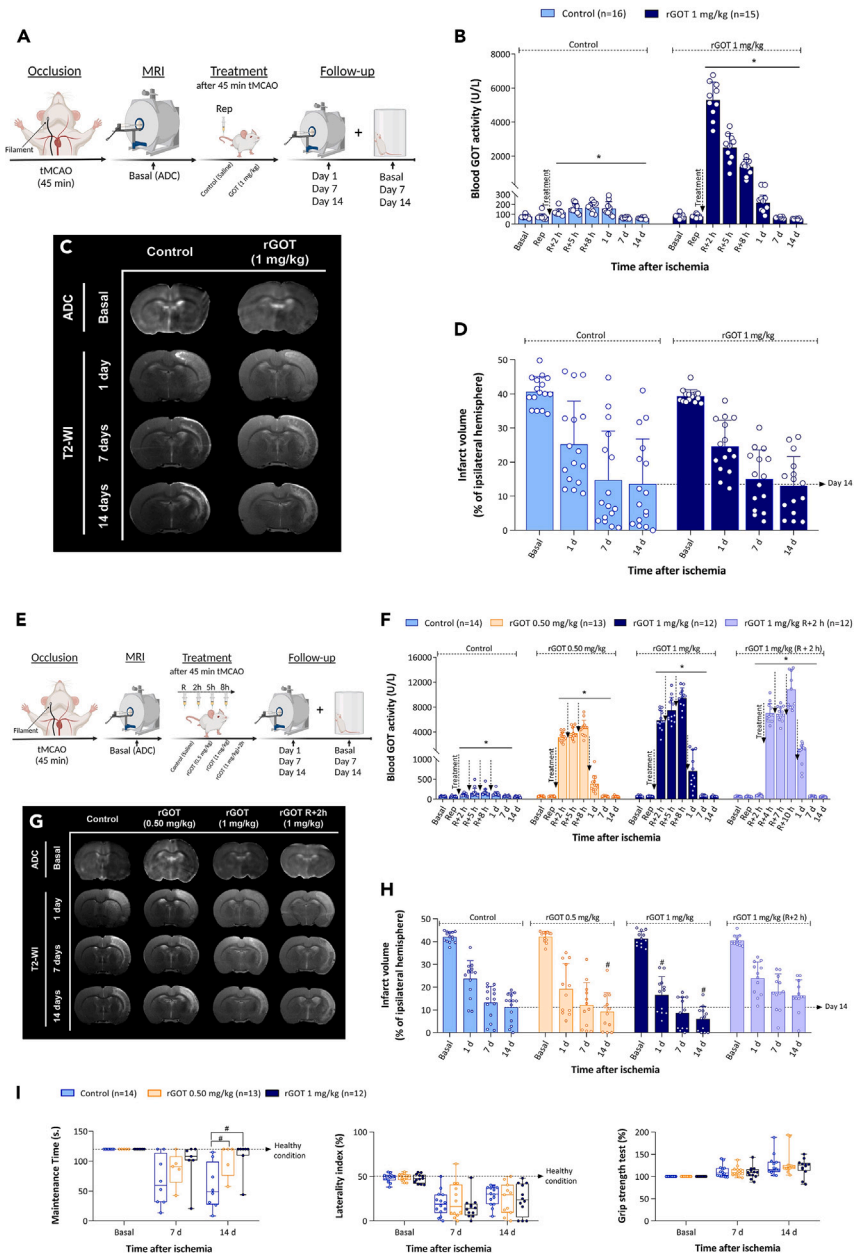

Figure 3. Therapeutic study of rGOT in rats with mild cerebral ischemia

(A) Schematic representation of the experimental design. Treatments (control and 1 mg/kg rGOT) were administered as a single i.v. bolus immediately after artery reperfusion (45 min after cerebral occlusion) in independent groups of ischemic animals. The ischemic lesion was measured using MRI at day 0 by ADC maps (during cerebral artery occlusion), and at days 1, 7, and 14 after ischemia induction by T2-maps. Basal lesion assessment at day 0 was used to confirm similar lesion volumes (35%–45%) in all included animals before treatment administration.

(B) Time course of blood GOT activity in ischemic rats.

(C) MRI analysis of the ischemic evolution.

(D) Infarct size assessment in ischemic rats. The ischemic lesion is represented as the percentage adjusted to the ipsilateral hemisphere. The dashed line represents the infarct volume at 14 days after ischemia in the control group (used as reference) to see the effects of treatments.

(E) Schematic representation of the experimental design. Treatments (control and rGOT 0.5 and 1 mg/kg) were administered (i.v.) in independent groups of ischemic animals four times over a period of 8 h. The first dose was initiated after artery reperfusion (45 min after cerebral occlusion), followed by three consecutive doses at 2, 5, and 8 h after artery reperfusion. A dose of 1 mg/kg administered 2 h after reperfusion was tested in an additional experimental group. The ischemic lesion was measured by MRI at day 0 by ADC maps (during cerebral artery occlusion), and at days 1, 7, and 14 after ischemia induction by T2-maps. Basal lesion assessment at day 0 was used to confirm similar lesion volumes (35%–45%) in all included animals before treatment administration.

Figure 3. *Continued*

Motor and somatosensory tests were evaluated by means of the rotarod test, cylinder test, and grip strength test 1 day before surgery (basal) and 7 and 14 days after ischemia.

(F) Time course of blood GOT activity in ischemic rats.

(G) MRI analysis of the ischemic evolution.

(H) Infarct size assessment in ischemic rats.

(I) Boxplots showing the assessment of sensorimotor function using the rotarod test (evaluated as maintenance time in seconds), cylinder test (evaluated as percentage of laterality), and grip strength (evaluated as percentage with respect to the basal condition). The dashed lines in the rotarod and cylinder tests represent the healthy condition of the animals before ischemic induction. In the grip strength test, a natural increase in muscular strength is reduced by an ischemic lesion. All data are expressed as mean ± standard deviation of the mean. p * <0.05 compared with the basal. p # < 0.05 compared with the control group at same time point. The data were analyzed using SPSS statistical software (v19.0) and GraphPad Prism software (v.8.3.0) for representation of graphs. The criterion for statistical significance was set at $p < 0.05$. The Shapiro–Wilk test was used to determine whether the data were normally distributed. Based on the results of normality tests and the sample size, statistical analysis was performed using non-parametric tests, Wilcoxon test for paired data, and Mann-Whitney test for unpaired data. ADC, apparent diffusion coefficient; i.v., intravenous; MRI, magnetic resonance imaging; R or Rep, reperfusion; tMCAO, transient middle cerebral artery occlusion; rGOT, recombinant glutamate-oxaloacetate transaminase; T2-WI, T2-weighted imaging. BioRender (https://biorender.com/) was used for creating the figures.

Consistent with our previous report,[21] one dose of 1 mg/kg rGOT-PEG increased GOT activity levels in the blood to over 4,000 U/L for at least 5 days, while basal GOT activity levels were recovered at 24 h for the rats receiving four doses of rGOT (Figure 4B). Protection efficacy, determined by infarct volume reduction, showed similar profiles at 7 and 14 days in both treatment groups (one dose of rGOT-PEG and four doses of rGOT) (Figures 4C and 4D).

In vitro and *in vivo* biocompatibility analysis between rGOT and the recombinant tissue plasminogen activator

Intravenous thrombolysis with alteplase® (recombinant tissue plasminogen activator, rtPA) is currently the only approved drug for acute ischemic stroke, with a maximum therapeutic time window of 4.5 h after the onset of stroke.[22] Considering that participants who received rtPA could be included in a future clinical trial with rGOT for acute stroke, an *in vitro* interaction assay to determine if its thrombolytic mechanism could be adversely affected by the rGOT drug candidate was first conducted. The results of the *in vitro* interaction (Figure 5A) demonstrated that the thrombolytic activity of rtPA was not affected by rGOT in a dose-dependent manner. Moreover, the enzymatic activity of rGOT was not affected by the proteolytic activity of rtPA (Figure 5B).

The interaction between rtPA and rGOT was later evaluated under *in vivo* conditions in healthy and ischemic animals. In both cases, two clinical situations were evaluated: the first situation was where rGOT was administered immediately in cases of suspected stroke before thrombolytic therapy, and the second was where both therapies were administered simultaneously, as illustrated in Figure 5C. In healthy animals, the increase in plasminogen activity after rtPA perfusion was not altered by rGOT treatment (Figure 5D). Similarly, the increase in GOT blood activity induced by the four doses of 1 mg/kg rGOT was not affected by rtPA in either clinical experimental approach (Figure 5E).

To analyze the treatment interaction of the two therapies in ischemic conditions, a thromboembolic rat model of MCAO (eMCAO) accepted to evaluate the recanalization effect of rtPA was used.[23,24] All animals included in this new analysis showed similar baseline lesion volumes before treatment administration (~48%). Only three animals (37.5% of the total) without recanalization therapy (control) showed transient events (less than 10 min) of spontaneous reperfusion. Meanwhile, in line with the experimental and clinical data,[25,26] complete or partial arterial reperfusion was observed in the three groups treated with rtPA (50%–60% reperfusion rate, Figure 5F). A mortality rate of 100% was observed at 24 h after ischemia (Figure 5G) in the control group with permanent occlusion, due to the massive ischemic lesion that this model causes. In contrast, the groups treated with rtPA alone or in combination with rGOT showed lower mortality rates (25% and 38%, respectively), which complement the previous analysis indicating that there is no interaction between both therapies. MRI analysis at 24 h in the three experimental groups (rtPA, $rGOT_{30\_min\_before}$ + rtPA, and rGOT + rtPA) revealed infarct volumes of 43% ± 2%, 43% ± 3%, and 38% ± 3% in the three groups, respectively (Figures 5H and 5I). Therefore, this analysis indicated that both treatments can be safely combined (individually or simultaneously) as thrombolytic and protective therapies.

Brain evaluation of rGOT-mediated protection

Blood glutamate levels were analyzed in parallel with GOT activity at the same time points in treated animals subjected to severe ischemia, with one and four doses of rGOT (Figure S6). Basal levels of glutamate in the blood ranged from 75 to 200 μM; however, the new form of rGOT did not affect the concentration of this metabolite at any dose tested. One possible reason for this could be the fast recovery of glutamate levels, in which any possible changes in glutamate levels were not detected at the selected blood sampling time points. To test this hypothesis, an artificial increase in blood glutamate levels to ~500 μM (from basal levels of ~100 μM) was induced in healthy rats by i.v. injection of a glutamate solution (1 mL, 1 M). Treatment with 1 mg/kg rGOT (tested before or after glutamate injection) did not modify the blood glutamate profile, which was analyzed every 10 min, as shown in Figure S7.

Non-invasive MR spectroscopy (MRS) was later used to monitor dynamic changes in metabolites in the brain and, more specifically, whether rGOT treatment could affect the levels of glutamate (Figure 6A), lactate (Figure 6B), and aspartate (Figure 6C). We conducted an analysis in a new set of ischemic rats (75 min after tMCAO) treated with saline (control group) or one dose of rGOT (1 or 4 mg/kg); this analysis revealed an immediate increase in the three metabolites after the ischemia onset, mainly during the occlusion period, and a decline following

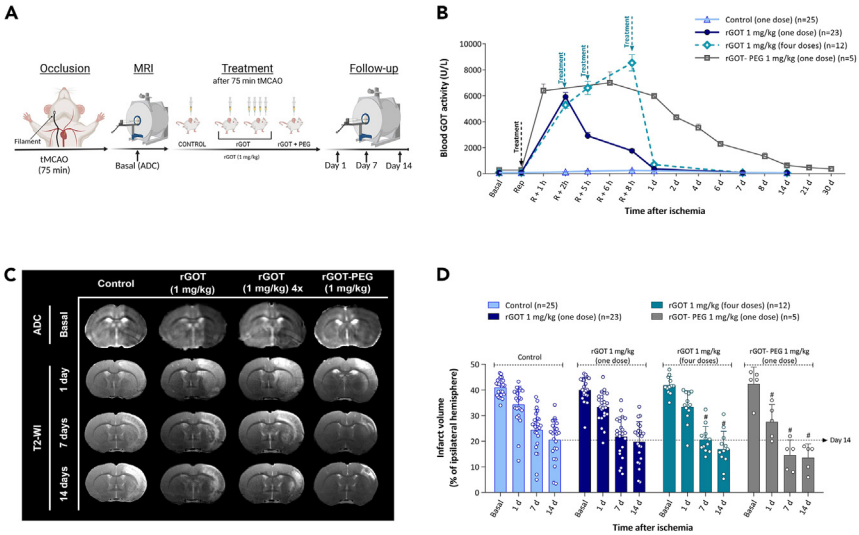

Figure 4. Therapeutic study of sustained rGOT-PEG activity in ischemic rats

(A) Schematic representation of the experimental design. Independent groups of ischemic animals were treated (i.v.) with saline (control), one dose of rGOT, four doses (defined as 4×) of rGOT, and one dose of rGOT-PEG (all doses 1 mg/kg of rGOT protein). All treatments were initiated immediately after artery reperfusion (75 min after cerebral occlusion). Four doses of rGOT were administered in a period of 8 h, with intervals of 2, 3, and 3 h after artery reperfusion. The ischemic lesion was measured by MRI at day 0 by ADC maps (during cerebral artery occlusion), and at days 1, 7, and 14 after ischemia induction by T2-maps. Basal lesion assessment at day 0 was used to confirm similar lesion volumes (35%–45%) in all included animals before treatment administration.

(B) Time course of blood GOT activity in ischemic rats.

(C) MRI analysis of the ischemic evolution.

(D) Infarct size assessment in ischemic rats. The ischemic lesion is represented as the percentage adjusted to the ipsilateral hemisphere. The dashed line represents the infarct volume of the control group at 14 days after ischemia (used as a reference) to see the effect of treatments. All data are expressed as mean ± standard deviation of the mean. p * <0.05 compared with the basal. p # < 0.05 compared with the control group at same time point. The data were analyzed using SPSS statistical software (v19.0) and GraphPad Prism software (v.8.3.0) for representation of graphs. The criterion for statistical significance was set at $p < 0.05$. The Shapiro–Wilk test was used to determine whether the data were normally distributed. Based on the results of normality tests and the sample size, statistical analysis was performed using non-parametric tests, Wilcoxon test for paired data, and Mann-Whitney test for unpaired data. ADC, apparent diffusion coefficient; i.v., intravenous; MRI, magnetic resonance imaging; R or Rep, reperfusion; tMCAO, transient middle cerebral artery occlusion; rGOT, recombinant glutamate-oxaloacetate transaminase; PEG, polyethylene glycol; T2-WI, T2-weighted imaging. BioRender (https://biorender.com/) was used for creating the figures.

reperfusion. This result is in line with the metabolic changes related to the ischemic cascade and agrees with other studies using MRS.[27–29] Intriguingly, treatment with rGOT did not show a clear or significant effect on the concentration profiles of these three metabolites compared with the control.

The lack of an effect of rGOT on blood and brain glutamate levels led to the hypothesis that rGOT could potentially reach the brain parenchyma and promote other neuroprotective pathways, which would challenge the currently hypothesized mechanism of action of rGOT. Cerebrospinal fluid (CSF) is directly linked to the central nervous tissue and therefore can be used to monitor drug penetration into the CNS.[30] We conducted a longitudinal assessment of GOT activity in the CSF of healthy and ischemic rats (75 min after tMCAO) treated with either saline (control), one dose of rGOT (1 and 4 mg/kg), or four doses of rGOT (1 mg/kg each). GOT activity was detected in the CSF under basal conditions with an average value of 12 ± 4 U/L (Figures 6D and 6F). The ischemic lesion in untreated animals caused an increase to 20 ± 3 U/L 2 h after lesion induction, likely due to brain cell damage and the release of the endogenous enzyme into the extracellular space (Figure 6F). In both healthy and ischemic animals, the increase in GOT activity in the CSF correlated with the dose of rGOT administered (Figures 6D and 6F), although the rate at which it increased was lower than that observed in the blood (Figures 6E and 6G).

Using quantitative liquid chromatography and tandem mass spectrometry (LC-MS/MS) with sequential window acquisition of all theoretical mass spectra (SWATH-MS) analysis in brain tissues, the diffusion of rGOT from the blood to the brain parenchyma was confirmed in healthy and ischemic animals treated with one dose of 1 mg/kg rGOT (Figure 6H). This increase correlated with the blood analysis in the same animals (Figure 6I).

The biodistribution of rGOT at the whole-body level was finally investigated in both control and tMCAO animals using positron emission tomography (PET) imaging. For this, animals were intravenously administered [^{18}F]rGOT (1 mg/kg), and dynamic images were acquired over 2 h. Images revealed an increased accumulation of [^{18}F]rGOT in the brain of diseased animals compared to aged-matched controls (Figures 6J–6L). Whole-body images of tMCAO animals confirmed slower kidney elimination, higher liver accumulation, and longer residence time of [^{18}F]rGOT in the blood (Figure S8).

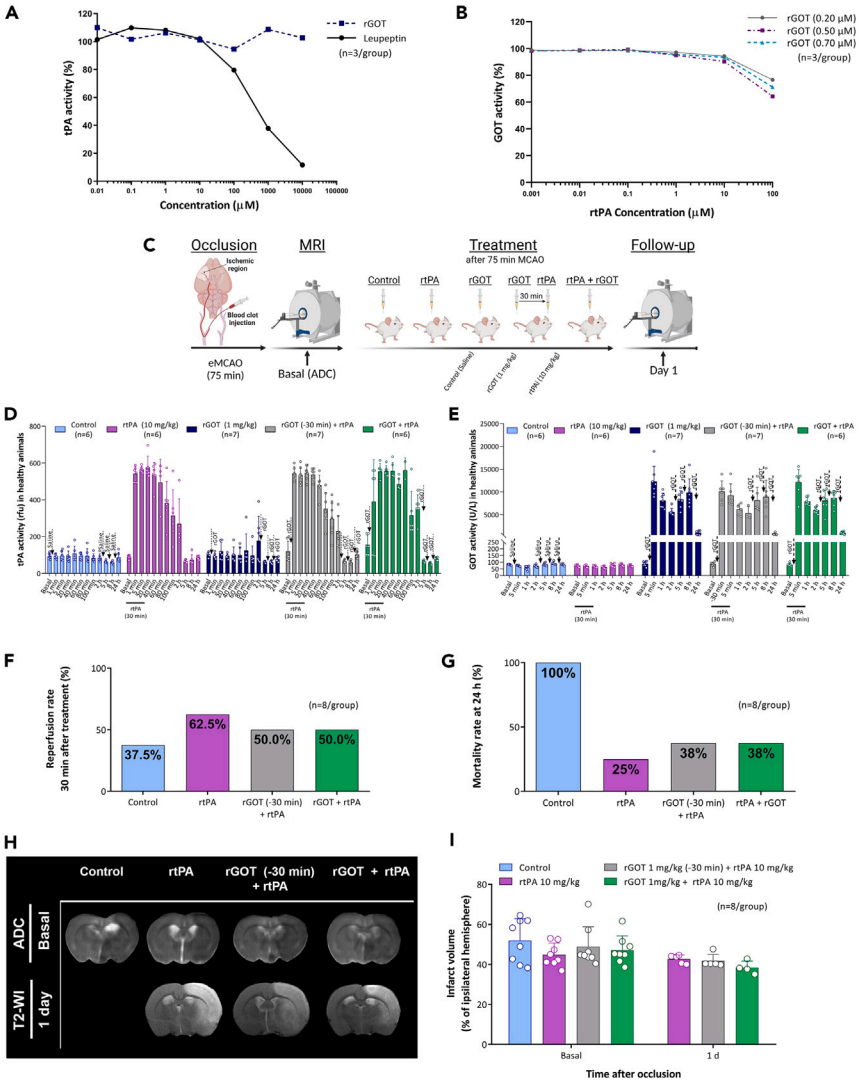

Figure 5. *In vitro* and *in vivo* interaction between rtPA and rGOT

(A) *In vitro* analysis of rtPA activity analyzed in combination with the increasing concentration of rGOT. Leupeptin was used as an inhibitor control of rtPA activity.

(B) *In vitro* analysis of rGOT activity determined in the presence of increasing concentrations of rtPA.

(C) Schematic representation of the experimental design of the interaction study between rtPA and rGOT in healthy and ischemic model induced by the thromboembolic occlusion of the MCAO (eMCAO). Independent groups of animals were treated with saline (control), rtPA 10 mg/kg (1 mL; 10% administered in an initial loading bolus, the other 90% of the dose was continuously infused), rGOT 1 mg/kg, rGOT 1 mg/kg treated simultaneously with rtPA 10 mg/kg, and a final group treated with rGOT 1 mg/kg 30 min before rtPA 10 mg/kg. The ischemic lesion was measured by MRI at day 0 by ADC maps (during cerebral artery occlusion, 75 min) and at day 1 by T2-maps. Basal lesion assessment at day 0 confirmed similar lesion volumes in all included animals before treatment administration.

(D) *In vivo* interaction of rtPA with rGOT (four doses of 1 mg/kg) activity and (E) interaction of rGOT (four doses of 1 mg/kg) with rtPA activity, in healthy animals. Blood levels of rtPA and GOT activity were determined in the blood before treatment administration (basal values), and 24 h after treatment.

(F) Reperfusion rate determined at 30 min after treatment administration. Successful reperfusion was considered to be when at least 40% of the basal cerebral blood flow was recovered within the first 40 min after treatment administration.

(G) Mortality rate (%) at 24 h after ischemic induction.

(H) MRI analysis of the ischemic evolution.

(I) Infarct size assessment in ischemic rats. Ischemic lesions are represented as the percentage adjusted to the ipsilateral hemisphere. All data are expressed as mean ± standard deviation of the mean. The data were analyzed using SPSS statistical software (v19.0) and GraphPad Prism software (v.8.3.0) for representation of graphs. BioRender (https://biorender.com/) was used for creating the figures. The criterion for statistical significance was set at $p < 0.05$. The Shapiro–Wilk test was used to determine whether the data were normally distributed. Based on the results of normality tests and the sample size, statistical analysis was performed using non-parametric tests, Wilcoxon test for paired data, and Mann-Whitney test for unpaired data. ADC, apparent diffusion coefficient; eMCAO, embolic middle cerebral artery occlusion rat model; i.v., intravenous; MRI, magnetic resonance imaging; rtPA, recombinant tissue plasminogen activator; R/Rep, reperfusion; rGOT, recombinant glutamate-oxaloacetate transaminase; T2-WI, T2-weighted imaging.

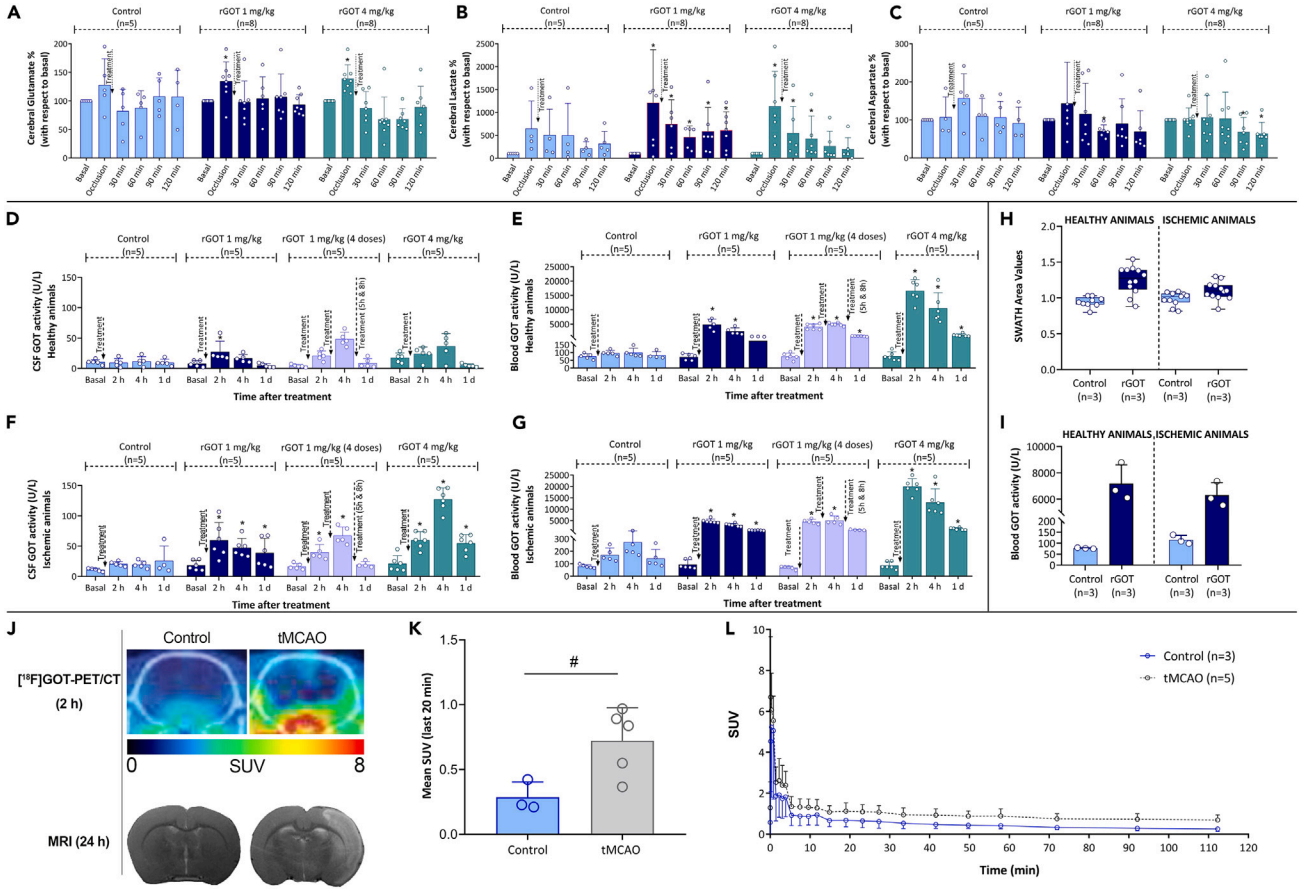

Figure 6. Analysis of rGOT treatment in the brain of healthy and ischemic animals

MRS analysis of (A) glutamate, (B) lactate, and (C) aspartate in independent groups of ischemic animals who underwent transient occlusion (75 min) of the middle cerebral artery. Treatments (saline, one dose of 1 and 4 mg/kg of rGOT) were initiated immediately after arterial perfusion. Metabolite levels were determined in basal conditions (before ischemic induction), during artery occlusion, and 30, 60, 90, and 120 min after reperfusion.

(D) Analysis of GOT activity in CSF and (E) blood samples from healthy animals treated (i.v.) with saline (control group), one dose of rGOT 1 mg/kg, four doses of rGOT 1 mg/kg, and one dose of rGOT 4 mg/kg. Levels of GOT were analyzed before treatment administration (basal levels) and 2, 4, and 24 h after treatment administration.

(F) Analysis of GOT activity in CSF and (G) blood samples from ischemic animals treated with saline (control group), one dose of rGOT 1 mg/kg, four doses of rGOT 1 mg/kg, and one dose of rGOT 4 mg/kg. Ischemic lesion was induced by the transient occlusion (75 min) of the middle cerebral artery. Treatments were initiated immediately after arterial perfusion. Levels of GOT were analyzed before ischemia, during artery occlusion (before reperfusion), and 2, 4, and 24 h after treatment administration.

(H) LC-MS/MS by sequential window acquisition of all theoretical mass spectra (SWATH-MS) analysis of GOT levels in brain tissue from healthy and ischemic animals (45 min of tMCAO) treated with saline (control) and one dose of rGOT 1 mg/kg. GOT was analyzed in the brain and blood (I) 1 h after treatment administration in the perfused brain tissues and blood, respectively.

(J) Evaluation of cerebral [18^F]GOT-PET signal uptake in healthy and ischemic rat brains at 2 h after i.v. treatment administration. The healthy brain in control and ischemic lesion in tMCAO animals was evaluated at 24 h using MRI. PET brain images of axial planes at the level of the ischemic lesion are co-registered with the CT of the same animal. The time-activity curve of the VOI placed on the whole brain of control and ischemic animals after i.v. administration of [18^F]GOT.

(K) Representation of mean SUV values of the last 20 min of PET acquisition in control and tMCAO rat brains.

(L) Values are presented as scatter dot blot. All data are expressed as mean ± standard deviation of the mean. p * <0.05 compared with the basal. p # < 0.05 compared with the control group at same time point. The data were analyzed using SPSS statistical software (v19.0) and GraphPad Prism software (v.8.3.0) for representation of graphs. The criterion for statistical significance was set at $p < 0.05$. The Shapiro–Wilk test was used to determine whether the data were normally distributed. Based on the results of normality tests and the sample size, statistical analysis was performed using non-parametric tests, Wilcoxon test for paired data, and Mann-Whitney test for unpaired data. CSF, cerebrospinal fluid; CT, computed tomography; i.v., intravenous; LC-MS/MS, liquid chromatography with tandem mass spectrometry; MRI, magnetic resonance imaging; MRS, magnetic resonance spectroscopy; PET, positron emission tomography; rGOT, recombinant glutamate-oxaloacetate transaminase; tMCAO, transient middle cerebral artery occlusion; SUV, standardized uptake values; VOI, volume of interest. BioRender (https://biorender.com/) was used for creating the figures.

Quantitative LC-MS/MS by SWATH-MS used to analyze GOT in the brain parenchyma is also a powerful technique to detect changes in protein expression affected by rGOT treatment. In this case, the protein expression profile in the brain of ischemic animals treated with saline was compared to that in animals treated with four doses of 1 mg/kg rGOT following the protocol indicated in Figure S9. Dysregulated proteins were identified when $p < 0.05$, and fold change > 1.5 or <0.8 was chosen as cutoffs. Eleven proteins were identified as being significantly dysregulated (six upregulated and five downregulated) in the treated animals compared with the control (Figures S10A and S10B). The upregulated and downregulated proteins were subjected to functional analysis using FunRich. From this analysis, the upregulated proteins were found to be mainly involved in metabolic processes, such as ATP biosynthesis, the glycolytic process, mitochondrial dynamics, NADH metabolism, and pyridoxal phosphate catabolism (represented in Figure S10C). The downregulated proteins were associated with other biological processes, including the glycerol-3-phosphate catabolic process, the glycerophosphate shuttle, and RNA transcription.

Analysis of *in vitro* neuronal protection of rGOT

Since we observed that rGOT was able to cross the blood-brain barrier after administration and induce changes in protein expression patterns, we scrutinized any direct protective effect of rGOT on neuronal cells that could justify the *in vivo* infarct volume reduction observed for treated ischemic animals. Protection analysis was evaluated in primary cortical neurons subjected to an ischemic model of oxygen-glucose deprivation (OGD) for 90 min and incubated for 24 h either in the absence or presence of increasing concentrations of rGOT. As shown in Figure 7A, rGOT protected neurons against OGD-induced neuronal apoptosis, as revealed by the decrease in both caspase-3 activation and the percentage of apoptotic neurons, indicated in Figure 7B. Interestingly, the neuroprotective effect of rGOT was evident at the lowest (1.8 μg/mL) concentration tested. Moreover, the neuroprotection provided by rGOT was even detected at higher concentrations of the enzyme, providing a wide therapeutic window. rGOT also prevented mitochondrial membrane potential depolarization in neurons caused by OGD and related to apoptotic death (Figure 7C).[31] *In vitro* rGOT protection was also independently analyzed by a second laboratory via cell viability under model glutamate excitotoxicity and OGD in HT-22 and SH-5YSY neuronal cell lines (Figure 7D). Exposing HT-22 cells to 20 mM glutamate for 5 h induced an approximate 40% reduction in cell viability. Replenishing the media with 10 μg/mL rGOT enhanced cell survival; however, the protective effect was not statistically significant. A 1.6-fold increase in the glutamate level was detected after induction of glutamate excitotoxicity, which was reduced to about the level of the control after rGOT exposure (Figure 7E). Similarly, exposing human neuroblastoma SH-SY5Y cells to 20 mM glutamate for 6 h reduced cell viability to 60%, and replenishing the media with rGOT significantly improved cell survival to 70%. Concomitantly, the glutamate level that increased 1.6-fold after glutamate excitotoxicity was significantly reduced to the level of the negative control. Subjecting the HT-22 cells to glutamate + OGD for 5 h significantly reduced cell viability to 64% in mouse hippocampal HT-22 cells, and following reperfusion with rGOT added to the culture media, viability significantly improved to 75%. The glutamate level in the HT-22 cell medium was significantly elevated by 1.5-fold compared to untreated cells, and reperfusion after OGD with rGOT reduced the glutamate level. Similarly, exposing human neuroblastoma SH-SY5Y cells to glutamate + OGD reduced cell viability to 67%, and reperfusion with rGOT improved cell survival to 85%. Additionally, the glutamate level measured after OGD exposure showed a significant 2.5-fold increase as compared to the untreated cells. Following reperfusion with rGOT, the glutamate level was significantly reduced again. These data clearly suggest that rGOT had a direct neuroprotective effect in both mouse hippocampal HT-22 and human neuroblastoma SH-SY5Y cells in response to glutamate excitotoxicity.

rGOT labeling with rhodamine used for *in vitro* imaging confocal tracking demonstrated a time-dependent uptake (tested from 1 to 24 h) of the enzyme in the primary culture neuronal cells (Figures 7F and 7G) and also in astrocytes (Figures 7H and 7I).

The finding that rGOT was uptaken by the cells led to the evaluation of whether it could cause any toxic effect on them. Four cell lines were used to test the cytotoxicity and genotoxicity of rGOT: human lymphoblastoid TK6, HT-22, SH-SY5Y, and human astrocytes cell lines (1321N1). No cytotoxicity (Figures S11A and S11B) or genotoxicity, by DNA strand breaks, (Figures S11C–S11F) was detected, respectively, in any of the cell lines after exposure to rGOT for 3 and 24 h. Chromosomal damage analyzed by micronuclei formation was not detected after the exposure of TK6 cells to rGOT (Figure S11G). GOT did not induce any mutagenic effect detected by the HPRT gene mutation assay in V79-4 cells, compared to the negative control (Figure S11H).

DNA double-strand breaks (DSBs) are one of the most deleterious lesions that can be induced by a genotoxic agent. Upon DSB formation, histone H2AX molecules are rapidly phosphorylated at serine 139 near the site of DNA DSBs, termed as γ-H2AX marks.[32] No induction of γ-H2AX foci was detected after neuronal HT-22, SH-SY5Y, and astrocytic 1321N1 cells exposed to 30 μg/mL rGOT (Figure S11I). The cells treated with positive control etoposide showed massive induction of γ-H2AX. Thus, no genotoxicity of rGOT was detected in any of the cell lines subjected to the genotoxicity tests (Figure S11J).

rGOT promotes autophagy during hypoxia-induced ER stress in neuronal cells

Autophagy is a critical and well-described mechanism that is activated by hypoxia and/or ischemia-reperfusion and contributes to the cell death/survival balance in ischemic lesions.[33–35] Therefore, we evaluated whether rGOT protection could mediate this phenomenon. We evaluated two modulators of autophagy during hypoxia: hypoxia-inducible factor-1 α (HIF1α) and endoplasmic reticulum (ER) stress.[36–38] As a model, we used HT-22 mouse hippocampal neuronal and SH-SY5Y human neuroblastoma cell lines. We identified that HIF1α prominently accumulated in both HT-22 and SH-SY5Y neuronal cells following hypoxia in comparison to the normoxic condition (Figure 8A). We observed that hypoxia caused significant accumulation of HIF1α that was abolished following reoxygenation in HT-22 and SH-SY5Y cell lines (Figure 8A). In this setup, we also tested the effect of rGOT (10 μg/mL) on HIF1α accumulation. The administration of rGOT partially or totally abolished the accumulation of HIF1α in HT-22 and SH-SY5H neuronal cell lines (Figure 8A). To analyze the function of HIF1α, we checked the transcription

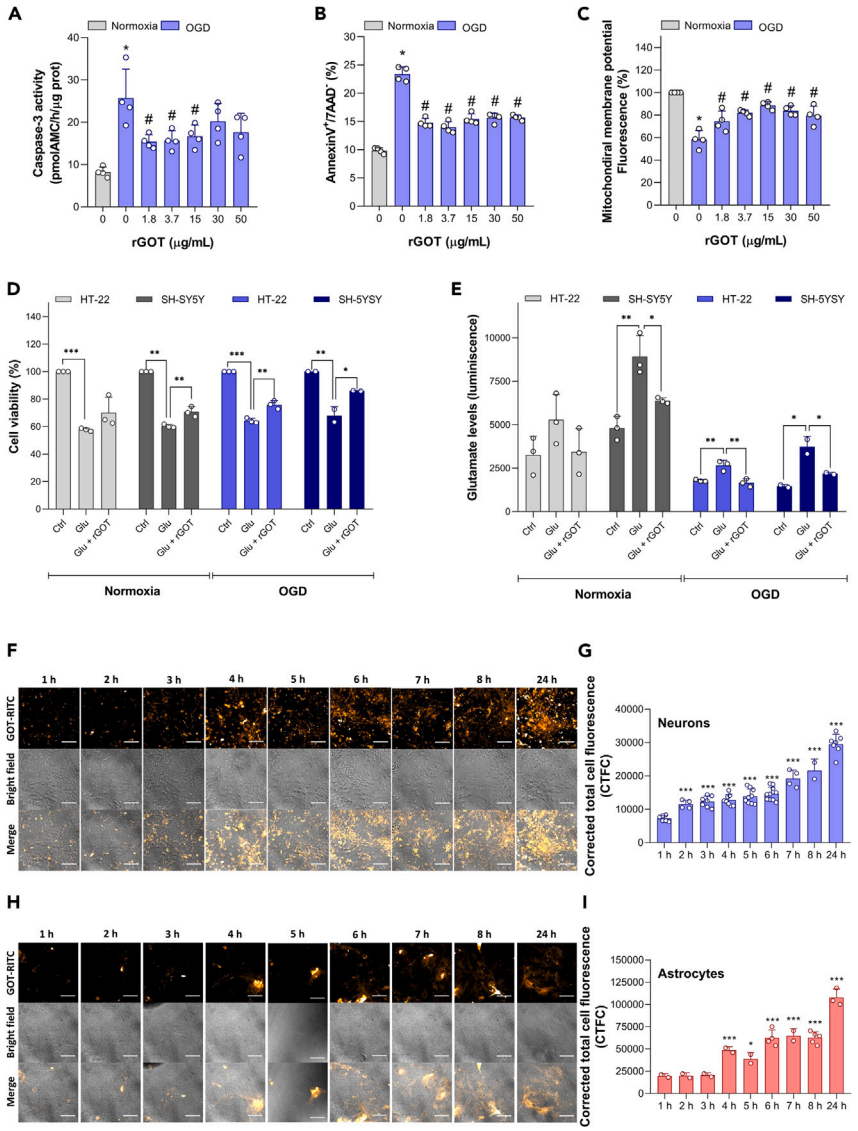

Figure 7. *In vitro* protection analysis of rGOT in neuronal cultures

(A) rGOT protection in primary neuronal culture. Neurons were subjected to normoxia or oxygen and glucose deprivation (OGD) conditions, for 90 min, and were further incubated in culture medium for 24 h, in the absence of presence of increasing concentrations of rGOT (1.8–50 µg/mL). Caspase-3 activity and (B) neuronal apoptosis (AnnexinV$^+$/7AAD$^-$ neurons) were analyzed by fluorimetry and flow cytometry, respectively.

(C) Mitochondrial depolarization was determined by flow cytometry. Data are represented as mean ± standard deviation from 4 different neuronal cultures (*$p < 0.05$ versus normoxia; #$p < 0.05$ versus OGD).

(D) Neuroprotective effect of rGOT upon glutamate excitotoxicity or OGD. Cell viability was measured by the AlamarBlue assay after exposure to 20 mM glutamate or glutamate and rGOT (10 µg/mL) for 5 or 6 h in HT-22 cells and SH-5YSY cell, respectively. OGD was induced during 5 h with or without rGOT (10 µg/mL) during reperfusion in the same cell lines.

(E) Glutamate levels were measured in parallel in HT-22 and SH-5YSY cells. As positive control, cells were treated with chlorpromazine hydrochloride (CHL, 50 µM), leading to 2%–10% viability (data not shown). Data are expressed as the average value of three independent experiment replicates ± standard deviation. One-way ANOVA followed by Bonferroni's multiple comparison test. *$p < 0.5$, **$p < 0.01$, ***$p < 0.001$; h, hours.

(F) Confocal images of cortical neuron primary cultures and (G) astrocyte primary cultures treated with GOT labeled with rhodamine B isothiocyanate (GOT-RITC). The incubation with the GOT-RITC was conducted during 1, 2, 3, 4, 5, 6, 7, 8, and 24 h to study the internalization throughout the hours. The quantification of the internalization in neurons (I) and astrocytes (H) was performed through corrected total cell fluorescence (CTCF). Scale bar: 50 µm. Purity of neuronal and astrocytes cultures is indicated in Figures S12 and S13 respectively. Data are represented as mean ± standard deviation (*$p < 0.05$; ***$p < 0.001$ versus 1 h). The data were analyzed using SPSS statistical software (v19.0) and GraphPad Prism software (v.8.3.0) for representation of graphs. CTCF, Ctrl, control; corrected total cell fluorescence; Glu, glutamate; OGD, oxygen and glucose deprivation; rGOT, recombinant glutamate-oxaloacetate transaminase.

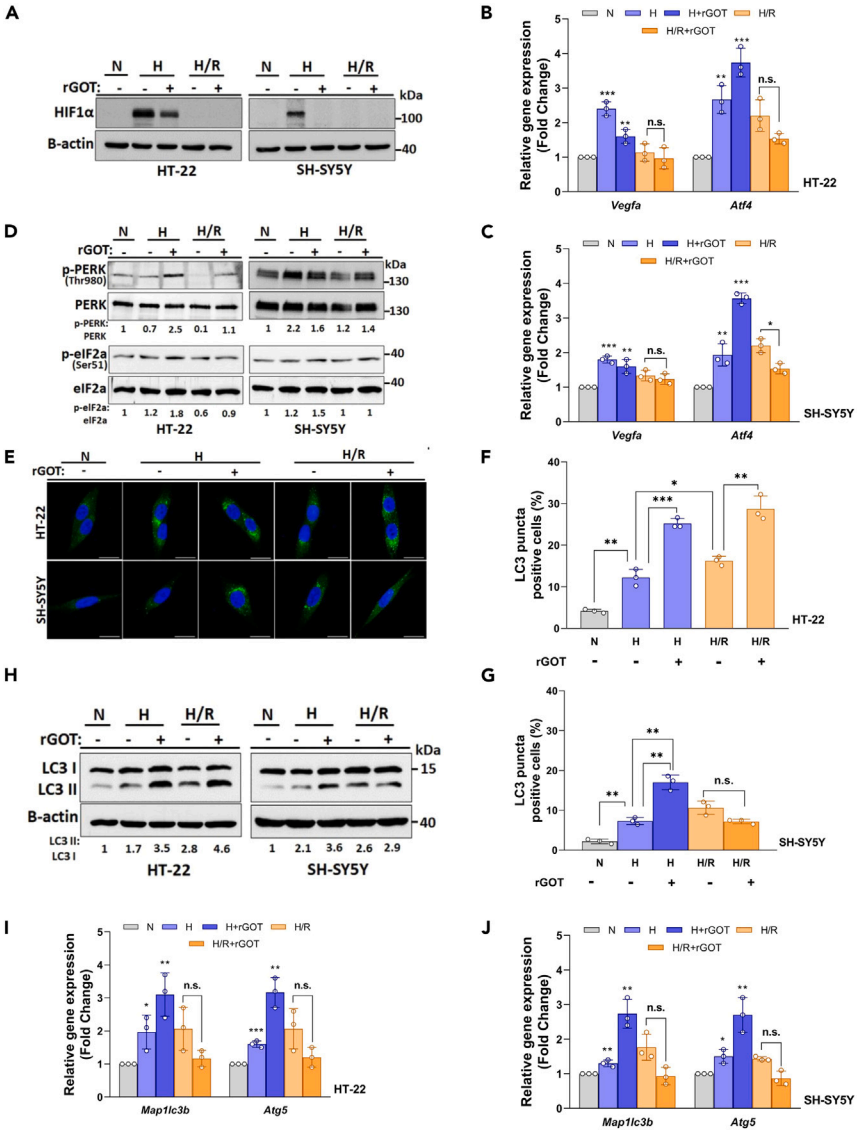

Figure 8. *In vitro* analysis of rGOT on autophagy in neuronal cultures

(A) HIF1α immunoblots of HT-22 and SH-SY5Y cells following hypoxia (H) and hypoxia/reoxygenation (H/R) with or without rGOT (10 μg/mL) treatment conditions. An anti-B-actin antibody was used as a loading control. Full western blots (WB) images are shown in Figure S14A.

(B and C) qRT-PCR analyses of *VEGFA* and *ATF4* mRNA expression levels following hypoxia (H) and hypoxia/reoxygenation (H/R) with or without rGOT (10 μg/mL) treatment conditions in both cell lines. GAPDH mRNA level was used as a control.

(D) Immunoblots of p-PERK and PERK, p-EIF2α and EIF2α following hypoxia (H) and hypoxia/reoxygenation (H/R) with or without rGOT (10 μg/mL) treatment conditions in both cell lines. ImageJ quantifications of p-PERK:PERK and p-eIF2a:eIF2a ratios were shown under the blots. Full WB images are shown in Figure S14B.

(E) LC3 (autophagy marker, green/Alexa 488) and DAPI (blue) were used to depict the nucleus staining following hypoxia (H) and hypoxia/reoxygenation (H/R) with or without rGOT (10 μg/mL) treatment conditions in both cell lines.

(F and G) Quantification and graphical representation of LC3 positivity. At least LC3 puncta of 150 cells were counted under each condition.

(H) Immunoblot analyses of LC3-shift assays following hypoxia (H) and hypoxia/reoxygenation (H/R) with or without rGOT (10 μg/mL) treatment conditions in both cell lines. β-actin was used as a loading control. ImageJ quantifications of LC3 II:LC3 I ratios were shown under the blots. Full WB images are shown in Figure S14C.

(I and J) qRT-PCR analyses of *MAP1LC3B* and *ATG5* mRNA expression levels following hypoxia (H) and hypoxia/reoxygenation (H/R) with or without rGOT (10 μg/mL) treatment conditions in both cell lines. GAPDH mRNA level was used as a control. Statistical analyses were performed using Student's two-tailed t test or ordinary one-way ANOVA. Data were presented as means ± standard deviation of ≥3 independent experiments. Values of $p < 0.05$ were considered as significant. ***: $p < 0.001$, **: $p < 0.01$, *: $p < 0.05$. The data were analyzed using SPSS statistical software (v19.0) and GraphPad Prism software (v.8.3.0) for representation of graphs. H, hypoxia; N, normoxia; R, reperfusion; rGOT, recombinant glutamate-oxaloacetate transaminase.

level of two oxidative stress mediators, *VEGFA* and *ATF4*.[39] While mRNAs of both genes can be directly controlled by HIF1α, ER stress was shown to improve ATF4 mRNA stability and translation.[40,41] Quantitative reverse-transcription PCR (qRT-PCR) was performed using RNA isolated from treated or control cells. Expression of both genes was significantly increased under the hypoxic condition in both cell lines (Figures 8B and 8C). Reoxygenation in both cell lines caused a decrease in *VEGFA* mRNA in comparison to their hypoxic counterparts, while *ATF4* levels were sustained (Figures 8B and 8C).

Moreover, we also wanted to check changes following rGOT administration. While the increase in the mRNA levels of *VEGFA* was sustained upon rGOT addition, a prominent increase in the mRNA level of *ATF4* was observed in both cell lines during hypoxia (Figures 8B and 8C). These results indicated that GOT might have an effect on hypoxia-induced cellular responses. We subsequently checked the status of ER stress response proteins, such as PRKR-like endoplasmic reticulum kinase (PERK), eukaryotic translation initiation factor 2, and subunit 1 α (eIF2α) under hypoxia and/or reoxygenation conditions. PERK is one of the major sensor proteins that detect protein folding in the ER.[42] Under these conditions, phosphorylation and activation of PERK causes phosphorylation of eIF2α and switches off cap-dependent translation and stimulates numerous stress resilience and survival-related effectors.[43] Therefore, we evaluated the phosphorylation status of both PERK and eIF2α in our model. We observed that there was some activation of ER stress under hypoxia in our system, and the addition of rGOT positively regulated ER stress responses indicated by phosphorylation of PERK and its target protein eIF2α (Figure 8D). Since *ATF4* is also downstream to the PERK/eIF2α pathway, these results might explain a further increase that was observed in *ATF4* mRNA levels upon rGOT addition (Figures 8B and 8C). Therefore, rGOT treatment alleviated hypoxia-associated responses, but on the other hand, also potentiated the survival-related ER stress response of cells.

Autophagy can be activated by both hypoxia and ER stress, and it is crucial for determining the cells' fate, including neuronal cells. Upon autophagic stimuli, soluble autophagy protein LC3 (MAP1LC3) is conjugated to phosphatidylethanolamine resulting in the formation of autophagosome-associated LC3-II.[44] LC3-II lipidation causes LC3 puncta formation and LC3 shift in immunoblots. These assays are used as markers of autophagic activity. In our system, we observed an accumulation of LC3 puncta in both cells following hypoxia (Figures 8E–8G). Reoxygenation further increased LC3 puncta formation in both cell lines. The presence of rGOT under hypoxia resulted in further accumulation of LC3, indicating further activation of autophagy in both cell lines (Figures 8E–8G). rGOT treatment further potentiated hypoxia/reoxygenation-induced autophagy in HT-22 cells, and the effect was not prominent in SH-SY5Y cells (Figures 8E–8G). To further validate these results, we performed immunoblotting analyses. Similar to confocal results, LC3-II formation was increased following hypoxia, and it was sustained following reoxygenation in both cell lines. rGOT treatment in this context further stimulated LC3-II formation in both cell lines. Upon reoxygenation, addition of rGOT increased (Figure 8F) or sustained (Figure 8G) autophagic activity. *ATF4* modulates autophagy transcriptionally by controlling the mRNA levels of *MAP1LC3B* and *ATG5*.[45] In our model, we also tested the expression of these autophagy-related mRNAs. In line with changes in *ATF4* expression (Figures 8B and 8C), mRNA levels of *MAP1LC3B* and *ATG5* were upregulated following hypoxia and/or reoxygenation (Figures 8I and 8J). rGOT treatment under hypoxia resulted in a further increase in autophagy-related mRNA expression. Yet, rGOT treatment of reoxygenated cells did not result in a significant change in mRNA levels in both cell lines (Figures 8I and 8J). All these results indicated that hypoxic stress induced autophagy in neuronal cells. rGOT treatment resulted in a further upregulation of survival-related autophagy through the ER-related PERK/eIF2a/ATF4-dependent pathway, leading to rGOT-dependent neuroprotective effects.

DISCUSSION

The preclinical analysis developed in this study provides strong evidence to suggest that the administration of a recombinant human-identical GOT enzyme could potentially become a useful pharmacological agent for neuroprotection after ischemic stroke.[15–17,46] This is indicated by the pharmacokinetics, safety, and protection analysis described in the following text.

Pharmacokinetic analysis of this new version of rGOT revealed a $T_{1/2}$ of 2 h in rats and 5 h in primates, returning to basal values within the first 24 h. From a clinical perspective, this characteristic reduces the potential risk of long-term adverse effects, which is associated with other failed drugs that initially had promising results.[47,48] It is also unlikely that the administration of rGOT will induce toxic effects in humans, as the levels of this enzyme vary widely among healthy human (7–45 U/L) and have been shown to increase >10-fold in patients with liver damage.[49] However, considering that GOT is a key enzyme involved in different pathways of cell metabolism, a safety analysis in the NHP models and neuronal cell lines was included in this study. Although a subsequent regulatory safety phase 1 trial in humans is now required, these results support the future biocompatibility of the therapy and that it may be a safe drug.

Once demonstrated the safety of the therapy and, in line with the new recommendations for neuroprotection assessments adapted to the new era of reperfusion therapies,[50] the protective efficacy was evaluated later in a variety of *in vivo* experimental conditions that reflect the clinical conditions encountered during the acute phase of stroke after arterial recanalization. This study established that four consecutive doses of 1 mg/kg rGOT administered during the first 8 h (beginning before 2 h after arterial reperfusion) were the most protective protocol in both mild and severe ischemia. In this regard, we have also shown that the use of rGOT-PEG bioconjugate, which extends the half-life of the therapy, could circumvent the need for four consecutive doses of rGOT.

Initially, due to safety reasons, the most common clinical trials investigating neuroprotection for stroke opted to initiate therapeutic intervention after hospital arrival and neuroimaging diagnostics; this significantly reduces drug efficacy, as the drugs are designed to interfere with the initial pathways of the ischemic cascade.[51] With a narrow therapeutic window of 2 h after reperfusion (~3 h if we consider the ischemic onset), it is recommended that rGOT therapy be initiated as soon as possible as prehospital therapy, in the ambulance or at an outlying hospital, even in cases of suspected ischemic stroke without previous imaging diagnosis. This recommendation

requires that the drug be highly safe and compatible with hemorrhagic conditions and reperfusion therapies, such as rtPA. For those cases with stroke hemorrhage, previous preclinical studies have demonstrated that rGOT does not interfere with hematoma lesions and outcomes.[18] Secondly, our interaction analysis between rGOT and rtPA demonstrated that both enzymes can be combined simultaneously without interfering with each other's activities. A lack of biocompatibility with reperfusion therapies is an important aspect that limits the development of new protective agents for acute stroke. For instance, nerinetide, a promising protective agent against glutamate excitotoxicity, is sensitive to proteolytic cleavage when administered after rtPA, and therefore loses its effects in patients receiving thrombolytic therapy.[52]

The reduction in blood and brain glutamate levels has been described as the main mechanism related to the protective effect of rGOT. Its blood glutamate scavenging and protective effects have been described[17] with a previous recombinant hexahistidine-tagged form produced in *Escherichia coli* using a single dose of 0.12 mg/kg rGOT. With this new human version, four doses of 1 mg/kg were required to obtain sufficient protection without affecting blood or brain glutamate levels. One of the most rational explanations that could justify this discrepancy between the two versions of the enzyme could be the hexahistidine tag, which may affect the protein's intrinsic activity, stability, or three-dimensional structure, as reported for other recombinant proteins.[53]

The lack of effect of rGOT on blood glutamate aimed to develop consecutive CSF, proteomic, and PET analyses, indicating that rGOT can reach the brain and induce a local protective effect. This finding is also in line with a recent study that described the capability of the blood transaminases (including GOT) to be actively transported by the blood-brain barrier,[54] providing insight into pathophysiological CNS-peripheral organ communication.

It is generally accepted that after cerebral vessel occlusion, the ischemic region can be divided into two regions, an inner core region characterized by immediate necrotic cell death within the first minutes after stroke and a potentially salvageable region surrounding the ischemic core, defined as the penumbra and associated with delayed death caused by cellular apoptosis and autophagy events.[55] To elucidate whether both processes might underlie the protective effects of the therapy, *in vitro* assays were developed in primary culture and neuronal cell lines. The results showed that rGOT acts directly on neuronal cells by both reducing apoptosis and inducing cytoprotective autophagy. Therefore, these results seem to indicate the ability of the enzyme to cross the blood-brain barrier and reach the brain, providing a direct protection to the ischemic.

In conclusion, our findings established that tissue neuroprotection and improved functional outcomes are achievable by rGOT treatment given early in the acute phase of ischemic stroke after reperfusion. A sustained increase (~100-fold) in GOT activity for at least 8 h was needed to achieve protection, and treatment needed to begin within the first 3 h after stroke, considering the ischemia onset. This indicates the importance of initiating rGOT administration as soon as possible and maintaining GOT activity either via consecutive injections, continuous perfusion, or possibly with the long-acting rGOT-PEG bioconjugate form. The analysis of toxicity in NHPs and the lack of interaction with rtPA support that rGOT can be safely used in patients suspected of having a stroke. Efforts must be made now to translate these findings to humans.

Limitations of the study

Although this study includes robust preclinical data that demonstrate the potential clinical value of rGOT therapy for stroke, some limitations need to be discussed. First, although our findings indicate that this therapy can be safely initiated even early after ischemic stroke onset, such as pre-hospital administration or prior to reperfusion therapies, treatment was only tested after recanalization. Considering the possibility of an immediate clinical validation, this administration protocol design was selected, as this approach is more feasible as a subsequent clinical trial design than clinical pre-hospital administration. Second, due to the high mortality that occurred with the eMCAO model, the additive effect of rGOT on rtPA was not detected. In this regard, alternative stroke models with lower mortality, such as the *in situ* thromboembolic model of the MCA in combination with rtPA,[56] would be more appropriate for this analysis. Finally, our findings suggest that rGOT is able to cross the blood-brain barrier after blood administration and exerts a direct protective effect on neurons by both reducing apoptosis and inducing cytoprotective autophagy. Further investigation is now required to address and clarify how a large protein such as GOT is able to reach the brain and modulate apoptosis and autophagy.

RESOURCE AVAILABILITY

Lead contact

Further information and requests for resources and reagents should be directed to and will be fulfilled by the lead contact, Dr. Francisco Campos (francisco.campos.pérez@sergas.es).

Materials availability

Human rGOT enzyme produced for this study was supplied by Prof. David Mirelman (david.mirelma@weizmann.ac.il). Details can be obtained from the lead contact upon request.

Data and code availability

- All data reported in this paper will be shared by the lead contact upon request.
- This paper does not report original code.
- Any additional information required to reanalyze the data reported in this paper is available from the lead contact upon request.

ACKNOWLEDGMENTS

This study was supported by the Instituto de Salud Carlos III_ICIII (grant numbers ICI19/00032, PI20/01014, AC19/00066, and the RICORS-ICITUS network: RD21/0006/0003), Xunta de Galicia (grant number IN607D2020/03), the European Union program FEDER, and the European Regional Development Fund. This study was partially supported under the framework of EuroNanoMed III. A.Z. acknowledges a doctoral scholarship from the INRS/Tunisian Ministry of Education. M.A.G. is a Research Scholar of the Fonds de Recherche du Québec Santé (FRQS, Canada). J.L. thanks the grant AEI-MICINN/PID2020-117656RB-I00. F.C., T.S., and M.G.-F. declare ISCIII Miguel Servet contracts (CPII19/00020, CPII17/00027, and CPII20/0002, respectively). M.P.-M. and A.d.S.-C. declare an ISCIII Sara Borrell contract (CD19/00033 and CD20/00054, respectively). A.M. declare a Ramon y Cajal contract (RYC-2017-22412). B.P. thanks the support of the European Research Council (starting grant #950421) and the Xunta de Galicia (ED431F 2021/02, 2023-PG056, and Centro Singular De Investigación de Galicia Accreditation 2019–2022 (#ED431G 2019/03).

We thank the late Dr. V. Teichberg for his contributions to the development of GOT as a therapy for brain ischemic damage.

AUTHOR CONTRIBUTIONS

Conceptualization and methodology, M.P.-M., A.D.-L., J.C., D.M., and F.C.; investigation and data curation, M.P.-M., A.D.-L., S.L.-A., S.B.B., E.L.-A., C.C.-P., M.C., A.B.-C., R.I.-R., M.d.P.C.-V., A.d.S.-C., A.Z., M.A.G., A.M., J.L., Y.A., D.G., C.R., A.A., M.M., E.P., B.P., N.E.Y., T.S., and E.R.-P.; formal analysis, A.E.-G.; resources, D.M. and A.R.; writing – original draft, M.P.-M. and F.C.; writing – review and editing, S.A., M.S.-C., M.G.-F., J.V., M.C., E.D.-T., T.S., and J.C.; visualization, M.P.-M., A.D.-L., and F.C.; supervision, project administration, and funding acquisition, F.C.

DECLARATION OF INTERESTS

The funding sponsors did not participate in the study design; collection, analysis, or interpretation of data; writing the report; or in the decision to submit the paper for publication. Preparation of the new version of identical human rGOT at Biotechpharma (Lithuania) was supported by a grant from Sun Pharma (Mumbai, India) to Prof. David Mirelman.

STAR★METHODS

Detailed methods are provided in the online version of this paper and include the following:

- KEY RESOURCES TABLE
- EXPERIMENTAL MODEL AND STUDY PARTICIPANT DETAILS
  - Rodent care and housing
  - Primate animal care and housing
  - Surgical procedures in rats
- METHOD DETAILS
  - rGOT manufacturing and characterization
  - tPA activity analysis
  - GOT activity analysis
  - Blood glutamate analysis
  - Magnetic resonance imaging and image analysis
  - Quantitative proteomic analysis using the SWATH approach in brain tissue
  - Radiolabeling
  - PET imaging studies
  - Motor and somatosensory tests
  - Apoptosis analysis of rGOT treatment in primary cortical neurons subjected to ischemic model of oxygen-glucose deprivation (OGD)
  - Cell protection analysis of rGOT treatment in cell lines submitted to OGD and glutamate excitotoxicity
  - *In vitro* cytotoxic and genotoxic analysis of rGOT
  - Cell uptake analysis of rGOT
  - Characterization of autophagy in HT22 and SH-SY5Y cells and rGOT interaction
- QUANTIFICATION AND STATISTICAL ANALYSIS

SUPPLEMENTAL INFORMATION

Supplemental information can be found online at https://doi.org/10.1016/j.isci.2024.111108.

Received: April 11, 2024
Revised: August 21, 2024
Accepted: October 2, 2024
Published: October 9, 2024

REFERENCES

1. Rej, R. (1979). Measurement of aspartate aminotransferase activity: effects of oxamate. Clin. Chem. *25*, 555–559.
2. Rej, R. (1978). Aspartate aminotransferase activity and isoenzyme proportions in human liver tissues. Clin. Chem. *24*, 1971–1979.
3. Abrego, J., Gunda, V., Vernucci, E., Shukla, S.K., King, R.J., Dasgupta, A., Goode, G., Murthy, D., Yu, F., and Singh, P.K. (2017). GOT1-mediated anaplerotic glutamine metabolism regulates chronic acidosis stress in pancreatic cancer cells. Cancer Lett. *400*, 37–46. https://doi.org/10.1016/j.canlet.2017.04.029.
4. Vijay Kumar, K.D.G. (2018). To Determine Alanine and Aspartate Transaminase Activity in Serum (Springer). https://doi.org/10.1007/978-981-10-8186-6_25.
5. Zhang, D., Xiao, M., Wang, L., and Jia, W. (2019). Blood-Based Glutamate Scavengers Reverse Traumatic Brain Injury-Induced Synaptic Plasticity Disruption by Decreasing Glutamate Level in Hippocampus Interstitial Fluid, but Not Cerebral Spinal Fluid. Neurotox. Res. *35*, 360–372. https://doi.org/10.1007/s12640-018-9961-8.
6. Gruenbaum, B.F., Kutz, R., Zlotnik, A., and Boyko, M. (2020). Blood glutamate scavenging as a novel glutamate-based therapeutic approach for post-stroke depression. Ther. Adv. Psychopharmacol. *10*, 2045125320903951. https://doi.org/10.1177/2045125320903951.

7. Ruban, A., Berkutzki, T., Cooper, I., Mohar, B., and Teichberg, V.I. (2012). Blood glutamate scavengers prolong the survival of rats and mice with brain-implanted gliomas. Invest. New Drugs *30*, 2226–2235. https://doi.org/10.1007/s10637-012-9799-5.
8. Zhang, D., Mably, A.J., Walsh, D.M., and Rowan, M.J. (2017). Peripheral Interventions Enhancing Brain Glutamate Homeostasis Relieve Amyloid beta- and TNFalpha-Mediated Synaptic Plasticity Disruption in the Rat Hippocampus. Cereb. Cortex *27*, 3724–3735. https://doi.org/10.1093/cercor/bhw193.
9. Ruban, A., Malina, K.C.K., Cooper, I., Graubardt, N., Babakin, L., Jona, G., and Teichberg, V.I. (2015). Combined Treatment of an Amyotrophic Lateral Sclerosis Rat Model with Recombinant GOT1 and Oxaloacetic Acid: A Novel Neuroprotective Treatment. Neurodegener. Dis. *15*, 233–242. https://doi.org/10.1159/000382034.
10. Castillo, J., Loza, M.I., Mirelman, D., Brea, J., Blanco, M., Sobrino, T., and Campos, F. (2016). A novel mechanism of neuroprotection: Blood glutamate grabber. J. Cereb. Blood Flow Metab. *36*, 292–301. https://doi.org/10.1177/0271678X15606721.
11. Khanna, S., Briggs, Z., and Rink, C. (2015). Inducible glutamate oxaloacetate transaminase as a therapeutic target against ischemic stroke. Antioxid. Redox Signal. *22*, 175–186. https://doi.org/10.1089/ars.2014.6106.
12. Boyko, M., Stepensky, D., Gruenbaum, B.F., Gruenbaum, S.E., Melamed, I., Ohayon, S., Glazer, M., Shapira, Y., and Zlotnik, A. (2012). Pharmacokinetics of glutamate-oxaloacetate transaminase and glutamate-pyruvate transaminase and their blood glutamate-lowering activity in naive rats. Neurochem. Res. *37*, 2198–2205. https://doi.org/10.1007/s11064-012-0843-9.
13. Boyko, M., Gruenbaum, S.E., Gruenbaum, B.F., Shapira, Y., and Zlotnik, A. (2014). Brain to blood glutamate scavenging as a novel therapeutic modality: a review. J. Neural. Transm. *121*, 971–979. https://doi.org/10.1007/s00702-014-1181-7.
14. Rink, C., Gnyawali, S., Peterson, L., and Khanna, S. (2011). Oxygen-inducible glutamate oxaloacetate transaminase as protective switch transforming neurotoxic glutamate to metabolic fuel during acute ischemic stroke. Antioxid. Redox Signal. *14*, 1777–1785. https://doi.org/10.1089/ars.2011.3930.
15. Rink, C., Gnyawali, S., Stewart, R., Teplitsky, S., Harris, H., Roy, S., Sen, C.K., and Khanna, S. (2017). Glutamate oxaloacetate transaminase enables anaplerotic refilling of TCA cycle intermediates in stroke-affected brain. FASEB J. *31*, 1709–1718. https://doi.org/10.1096/fj.201601033R.
16. Xu, J., Khoury, N., Jackson, C.W., Escobar, I., Stegelmann, S.D., Dave, K.R., and Perez-Pinzon, M.A. (2020). Ischemic Neuroprotectant PKCepsilon Restores Mitochondrial Glutamate Oxaloacetate Transaminase in the Neuronal NADH Shuttle after Ischemic Injury. Transl. Stroke Res. *11*, 418–432. https://doi.org/10.1007/s12975-019-00729-4.
17. Perez-Mato, M., Ramos-Cabrer, P., Sobrino, T., Blanco, M., Ruban, A., Mirelman, D., Menendez, P., Castillo, J., and Campos, F. (2014). Human recombinant glutamate oxaloacetate transaminase 1 (GOT1) supplemented with oxaloacetate induces a protective effect after cerebral ischemia. Cell Death Dis. *5*, e992. https://doi.org/10.1038/cddis.2013.507.
18. Dopico-Lopez, A., Perez-Mato, M., da Silva-Candal, A., Iglesias-Rey, R., Rabinkov, A., Bugallo-Casal, A., Sobrino, T., Mirelman, D., Castillo, J., and Campos, F. (2021). Inhibition of endogenous blood glutamate oxaloacetate transaminase enhances the ischemic damage. Transl. Res. J. Lab. Clin. Med. *230*, 68–81. https://doi.org/10.1016/j.trsl.2020.10.004.
19. Campos, F., Rodríguez-Yáñez, M., Castellanos, M., Arias, S., Pérez-Mato, M., Sobrino, T., Blanco, M., Serena, J., and Castillo, J. (2011). Blood levels of glutamate oxaloacetate transaminase are more strongly associated with good outcome in acute ischaemic stroke than glutamate pyruvate transaminase levels. Clin. Sci. *121*, 11–17. https://doi.org/10.1042/CS20100427.
20. Campos, F., Sobrino, T., Ramos-Cabrer, P., Castellanos, M., Blanco, M., Rodríguez-Yáñez, M., Serena, J., Leira, R., and Castillo, J. (2011). High blood glutamate oxaloacetate transaminase levels are associated with good functional outcome in acute ischemic stroke. J. Cereb. Blood Flow Metab. *31*, 1387–1393. https://doi.org/10.1038/jcbfm.2011.4.
21. Zaghmi, A., Dopico-López, A., Pérez-Mato, M., Iglesias-Rey, R., Hervella, P., Greschner, A.A., Bugallo-Casal, A., da Silva, A., Gutiérrez-Fernández, M., Castillo, J., et al. (2020). Sustained blood glutamate scavenging enhances protection in ischemic stroke. Commun. Biol. *3*, 729. https://doi.org/10.1038/s42003-020-01406-1.
22. Hacke, W., Kaste, M., Bluhmki, E., Brozman, M., Dávalos, A., Guidetti, D., Larrue, V., Lees, K.R., Medeghri, Z., Machnig, T., et al. (2008). Thrombolysis with alteplase 3 to 4.5 hours after acute ischemic stroke. N. Engl. J. Med. *359*, 1317–1329. https://doi.org/10.1056/NEJMoa0804656.
23. Toomey, J.R., Valocik, R.E., Koster, P.F., Gabriel, M.A., McVey, M., Hart, T.K., Ohlstein, E.H., Parsons, A.A., and Barone, F.C. (2002). Inhibition of factor IX(a) is protective in a rat model of thromboembolic stroke. Stroke *33*, 578–585. https://doi.org/10.1161/hs0202.102950.
24. Alonso de Lecinana, M., Gutierrez, M., Roda, J.M., Carceller, F., and Diez-Tejedor, E. (2006). Effect of combined therapy with thrombolysis and citicoline in a rat model of embolic stroke. J. Neurol. Sci. *247*, 121–129. https://doi.org/10.1016/j.jns.2006.03.022.
25. Menon, B.K., Al-Ajlan, F.S., Najm, M., Puig, J., Castellanos, M., Dowlatshahi, D., Calleja, A., Sohn, S.I., Ahn, S.H., Poppe, A., et al. (2018). Association of Clinical, Imaging, and Thrombus Characteristics With Recanalization of Visible Intracranial Occlusion in Patients With Acute Ischemic Stroke. JAMA *320*, 1017–1026. https://doi.org/10.1001/jama.2018.12498.
26. Orset, C., Haelewyn, B., Allan, S.M., Ansar, S., Campos, F., Cho, T.H., Durand, A., El Amki, M., Fatar, M., Garcia-Yébenes, I., et al. (2016). Efficacy of Alteplase in a Mouse Model of Acute Ischemic Stroke: A Retrospective Pooled Analysis. Stroke *47*, 1312–1318. https://doi.org/10.1161/STROKEAHA.116.012238.
27. Baranovicova, E., Hnilicova, P., Kalenska, D., Kaplan, P., Kovalska, M., Tatarkova, Z., Tomascova, A., and Lehotsky, J. (2022). Metabolic Changes Induced by Cerebral Ischemia, the Effect of Ischemic Preconditioning, and Hyperhomocysteinemia. Biomolecules *12*, 554. https://doi.org/10.3390/biom12040554.
28. Nishizawa, Y. (2001). Glutamate release and neuronal damage in ischemia. Life Sci. *69*, 369–381. https://doi.org/10.1016/s0024-3205(01)01142-0.
29. Harada, K., Honmou, O., Liu, H., Bando, M., Houkin, K., and Kocsis, J.D. (2007). Magnetic resonance lactate and lipid signals in rat brain after middle cerebral artery occlusion model. Brain Res. *1134*, 206–213. https://doi.org/10.1016/j.brainres.2006.11.075.
30. Dembo, G., Park, S.B., and Kharasch, E.D. (2005). Central nervous system concentrations of cyclooxygenase-2 inhibitors in humans. Anesthesiology *102*, 409–415. https://doi.org/10.1097/00000542-200502000-00026.
31. Sanchez-Moran, I., Rodriguez, C., Lapresa, R., Agulla, J., Sobrino, T., Castillo, J., Bolanos, J.P., and Almeida, A. (2020). Nuclear WRAP53 promotes neuronal survival and functional recovery after stroke. Sci. Adv. *6*, eabc5702. https://doi.org/10.1126/sciadv.abc5702.
32. Keogh, M.C., Kim, J.A., Downey, M., Fillingham, J., Chowdhury, D., Harrison, J.C., Onishi, M., Datta, N., Galicia, S., Emili, A., et al. (2006). A phosphatase complex that dephosphorylates gammaH2AX regulates DNA damage checkpoint recovery. Nature *439*, 497–501. https://doi.org/10.1038/nature04384.
33. Rami, A., and Kögel, D. (2008). Apoptosis meets autophagy-like cell death in the ischemic penumbra: Two sides of the same coin? Autophagy *4*, 422–426. https://doi.org/10.4161/auto.5778.
34. Nabavi, S.F., Sureda, A., Sanches-Silva, A., Pandima Devi, K., Ahmed, T., Shahid, M., Sobarzo-Sánchez, E., Dacrema, M., Daglia, M., Braidy, N., et al. (2019). Novel therapeutic strategies for stroke: The role of autophagy. Crit. Rev. Clin. Lab Sci. *56*, 182–199. https://doi.org/10.1080/10408363.2019.1575333.
35. Lu, X., Zhang, J., Ding, Y., Wu, J., and Chen, G. (2022). Novel Therapeutic Strategies for Ischemic Stroke: Recent Insights into Autophagy. Oxid. Med. Cell. Longev. *2022*, 3450207. https://doi.org/10.1155/2022/3450207.
36. Buchberger, A., Bukau, B., and Sommer, T. (2010). Protein quality control in the cytosol and the endoplasmic reticulum: brothers in arms. Mol. Cell *40*, 238–252. https://doi.org/10.1016/j.molcel.2010.10.001.
37. Carloni, S., Albertini, M.C., Galluzzi, L., Buonocore, G., Proietti, F., and Balduini, W. (2014). Increased autophagy reduces endoplasmic reticulum stress after neonatal hypoxia-ischemia: role of protein synthesis and autophagic pathways. Exp. Neurol. *255*, 103–112. https://doi.org/10.1016/j.expneurol.2014.03.002.
38. Brocato, J., Chervona, Y., and Costa, M. (2014). Molecular responses to hypoxia-inducible factor 1alpha and beyond. Mol. Pharmacol. *85*, 651–657. https://doi.org/10.1124/mol.113.089623.
39. Pereira, E.R., Frudd, K., Awad, W., and Hendershot, L.M. (2014). Endoplasmic reticulum (ER) stress and hypoxia response pathways interact to potentiate hypoxia-inducible factor 1 (HIF-1) transcriptional activity on targets like vascular endothelial growth factor (VEGF). J. Biol. Chem. *289*, 3352–3364. https://doi.org/10.1074/jbc.M113.507194.

40. Vattem, K.M., and Wek, R.C. (2004). Reinitiation involving upstream ORFs regulates ATF4 mRNA translation in mammalian cells. Proc. Natl. Acad. Sci. USA *101*, 11269–11274. https://doi.org/10.1073/pnas.0400541101.
41. Gardner, L.B. (2008). Hypoxic inhibition of nonsense-mediated RNA decay regulates gene expression and the integrated stress response. Mol. Cell Biol. *28*, 3729–3741. https://doi.org/10.1128/MCB.02284-07.
42. Wang, P., Li, J., Tao, J., and Sha, B. (2018). The luminal domain of the ER stress sensor protein PERK binds misfolded proteins and thereby triggers PERK oligomerization. J. Biol. Chem. *293*, 4110–4121. https://doi.org/10.1074/jbc.RA117.001294.
43. Marciniak, S.J., Garcia-Bonilla, L., Hu, J., Harding, H.P., and Ron, D. (2006). Activation-dependent substrate recruitment by the eukaryotic translation initiation factor 2 kinase PERK. J. Cell Biol. *172*, 201–209. https://doi.org/10.1083/jcb.200508099.
44. Tanida, I., Mizushima, N., Kiyooka, M., Ohsumi, M., Ueno, T., Ohsumi, Y., and Kominami, E. (1999). Apg7p/Cvt2p: A novel protein-activating enzyme essential for autophagy. Mol. Biol. Cell *10*, 1367–1379. https://doi.org/10.1091/mbc.10.5.1367.
45. Rouschop, K.M.A., van den Beucken, T., Dubois, L., Niessen, H., Bussink, J., Savelkouls, K., Keulers, T., Mujcic, H., Landuyt, W., Voncken, J.W., et al. (2010). The unfolded protein response protects human tumor cells during hypoxia through regulation of the autophagy genes MAP1LC3B and ATG5. J. Clin. Invest. *120*, 127–141. https://doi.org/10.1172/JCI40027.
46. Teichberg, V.I., Cohen-Kashi-Malina, K., Cooper, I., and Zlotnik, A. (2009). Homeostasis of glutamate in brain fluids: an accelerated brain-to-blood efflux of excess glutamate is produced by blood glutamate scavenging and offers protection from neuropathologies. Neuroscience *158*, 301–308. https://doi.org/10.1016/j.neuroscience.2008.02.075.
47. Jia, M., Njapo, S.A.N., Rastogi, V., and Hedna, V.S. (2015). Taming glutamate excitotoxicity: strategic pathway modulation for neuroprotection. CNS Drugs *29*, 153–162. https://doi.org/10.1007/s40263-015-0225-3.
48. Chamorro, Á., Dirnagl, U., Urra, X., and Planas, A.M. (2016). Neuroprotection in acute stroke: targeting excitotoxicity, oxidative and nitrosative stress, and inflammation. Lancet Neurol. *15*, 869–881. https://doi.org/10.1016/S1474-4422(16)00114-9.
49. Tian, Z., Liu, H., Su, X., Fang, Z., Dong, Z., Yu, C., and Luo, K. (2012). Role of elevated liver transaminase levels in the diagnosis of liver injury after blunt abdominal trauma. Exp. Ther. Med. *4*, 255–260. https://doi.org/10.3892/etm.2012.575.
50. Savitz, S.I., Baron, J.C., Yenari, M.A., Sanossian, N., and Fisher, M. (2017). Reconsidering Neuroprotection in the Reperfusion Era. Stroke *48*, 3413–3419. https://doi.org/10.1161/STROKEAHA.117.017283.
51. Grupke, S., Hall, J., Dobbs, M., Bix, G.J., and Fraser, J.F. (2015). Understanding history, and not repeating it. Neuroprotection for acute ischemic stroke: from review to preview. Clin. Neurol. Neurosurg. *129*, 1–9. https://doi.org/10.1016/j.clineuro.2014.11.013.
52. Mayor-Nunez, D., Ji, Z., Sun, X., Teves, L., Garman, J.D., and Tymianski, M. (2021). Plasmin-resistant PSD-95 inhibitors resolve effect-modifying drug-drug interactions between alteplase and nerinetide in acute stroke. Sci. Transl. Med. *13*, eabb1498. https://doi.org/10.1126/scitranslmed.abb1498.
53. Booth, W.T., Schlachter, C.R., Pote, S., Ussin, N., Mank, N.J., Klapper, V., Offermann, L.R., Tang, C., Hurlburt, B.K., and Chruszcz, M. (2018). Impact of an N-terminal Polyhistidine Tag on Protein Thermal Stability. ACS Omega *3*, 760–768. https://doi.org/10.1021/acsomega.7b01598.
54. Sato, K., Tachikawa, M., Watanabe, M., Miyauchi, E., Uchida, Y., and Terasaki, T. (2019). Identification of Blood-Brain Barrier-Permeable Proteins Derived from a Peripheral Organ: In Vivo and in Vitro Evidence of Blood-to-Brain Transport of Creatine Kinase. Mol. Pharm. *16*, 247–257. https://doi.org/10.1021/acs.molpharmaceut.8b00975.
55. Moskowitz, M.A., Lo, E.H., and Iadecola, C. (2010). The science of stroke: mechanisms in search of treatments. Neuron *67*, 181–198. https://doi.org/10.1016/j.neuron.2010.07.002.
56. Correa-Paz, C., Perez-Mato, M., Bellemain-Sagnard, M., Gonzalez-Dominguez, M., Marie, P., Perez-Gayol, L., Lopez-Arias, E., Del Pozo-Filiu, L., Lopez-Amoedo, S., Bugallo-Casal, A., et al. (2024). Pharmacological preclinical comparison of tenecteplase and alteplase for the treatment of acute stroke. J. Cereb. Blood Flow Metab. *44*, 1306. https://doi.org/10.1177/0271678X241237427.
57. Stroke Therapy Academic Industry, R. (1999). Recommendations for standards regarding preclinical neuroprotective and restorative drug development. Stroke *30*, 2752–2758. https://doi.org/10.1161/01.str.30.12.2752.
58. Fernandez-Susavila, H., Iglesias-Rey, R., Dopico-Lopez, A., Perez-Mato, M., Sobrino, T., Castillo, J., and Campos, F. (2017). Inclusion criteria update for the rat intraluminal ischaemic model for preclinical studies. Dis. Models Mech. *10*, 1433–1438. https://doi.org/10.1242/dmm.029868.
59. Vieites-Prado, A., Iglesias-Rey, R., Fernández-Susavila, H., da Silva-Candal, A., Rodríguez-Castro, E., Gröhn, O.H.J., Wellmann, S., Sobrino, T., Castillo, J., and Campos, F. (2016). Protective Effects and Magnetic Resonance Imaging Temperature Mapping of Systemic and Focal Hypothermia in Cerebral Ischemia. Stroke *47*, 2386–2396. https://doi.org/10.1161/STROKEAHA.116.014067.
60. Overgaard, K., Sereghy, T., Boysen, G., Pedersen, H., Høyer, S., and Diemer, N.H. (1992). A rat model of reproducible cerebral infarction using thrombotic blood clot emboli. J. Cereb. Blood Flow Metab. *12*, 484–490. https://doi.org/10.1038/jcbfm.1992.66.
61. Pegg, C.C., He, C., Stroink, A.R., Kattner, K.A., and Wang, C.X. (2010). Technique for collection of cerebrospinal fluid from the cisterna magna in rat. J. Neurosci. Methods *187*, 8–12. https://doi.org/10.1016/j.jneumeth.2009.12.002.
62. Peroutka Iii, R.J., Orcutt, S.J., Strickler, J.E., and Butt, T.R. (2011). SUMO fusion technology for enhanced protein expression and purification in prokaryotes and eukaryotes. Methods Mol. Biol. *705*, 15–30. https://doi.org/10.1007/978-1-61737-967-3_2.
63. Butt, T.R., Edavettal, S.C., Hall, J.P., and Mattern, M.R. (2005). SUMO fusion technology for difficult-to-express proteins. Protein Expr. Purif. *43*, 1–9. https://doi.org/10.1016/j.pep.2005.03.016.
64. Bonzon-Kulichenko, E., Pérez-Hernández, D., Núñez, E., Martínez-Acedo, P., Navarro, P., Trevisan-Herraz, M., Ramos, M.d.C., Sierra, S., Martínez-Martínez, S., Ruiz-Meana, M., et al. (2011). A robust method for quantitative high-throughput analysis of proteomes by 18O labeling. Mol. Cell. Proteomics *10*, M110.003335. https://doi.org/10.1074/mcp.M110.003335.
65. Perez-Hernandez, D., Gutiérrez-Vázquez, C., Jorge, I., López-Martín, S., Ursa, A., Sánchez-Madrid, F., Vázquez, J., and Yáñez-Mó, M. (2013). The intracellular interactome of tetraspanin-enriched microdomains reveals their function as sorting machineries toward exosomes. J. Biol. Chem. *288*, 11649–11661. https://doi.org/10.1074/jbc.M112.445304.
66. Shevchenko, A., Wilm, M., Vorm, O., Jensen, O.N., Podtelejnikov, A.V., Neubauer, G., Shevchenko, A., Mortensen, P., and Mann, M. (1996). A strategy for identifying gel-separated proteins in sequence databases by MS alone. Biochem. Soc. Trans. *24*, 893–896. https://doi.org/10.1042/bst0240893.
67. Gonzalez-Rellan, M.J., Fondevila, M.F., Fernandez, U., Rodríguez, A., Varela-Rey, M., Veyrat-Durebex, C., Seoane, S., Bernardo, G., Lopitz-Otsoa, F., Fernández-Ramos, D., et al. (2021). O-GlcNAcylated p53 in the liver modulates hepatic glucose production. Nat. Commun. *12*, 5068. https://doi.org/10.1038/s41467-021-25390-0.
68. Lopez-Lopez, M., Regueiro, U., Bravo, S.B., Chantada-Vazquez, M.D.P., Varela-Fernandez, R., Avila-Gomez, P., Hervella, P., and Lema, I. (2021). Tear Proteomics in Keratoconus: A Quantitative SWATH-MS Analysis. Invest. Ophthalmol. Vis. Sci. *62*, 30. https://doi.org/10.1167/iovs.62.10.30.
69. Penas-Martinez, J., Barrachina, M.N., Cuenca-Zamora, E.J., Luengo-Gil, G., Bravo, S.B., Caparros-Perez, E., Teruel-Montoya, R., Eliseo-Blanco, J., Vicente, V., Garcia, A., et al. (2021). Qualitative and Quantitative Comparison of Plasma Exosomes from Neonates and Adults. Intern. J. Mol. Sci. *22*, 1926. https://doi.org/10.3390/ijms22041926.
70. Shilov, I.V., Seymour, S.L., Patel, A.A., Loboda, A., Tang, W.H., Keating, S.P., Hunter, C.L., Nuwaysir, L.M., and Schaeffer, D.A. (2007). The Paragon Algorithm, a next generation search engine that uses sequence temperature values and feature probabilities to identify peptides from tandem mass spectra. Mol. Cell. Proteomics *6*, 1638–1655. https://doi.org/10.1074/mcp.T600050-MCP200.
71. Ferreira, J.A. (2007). The Benjamini-Hochberg method in the case of discrete test statistics. Int. J. Biostat. *3*, 11. https://doi.org/10.2202/1557-4679.1065.
72. Pathan, M., Keerthikumar, S., Ang, C.S., Gangoda, L., Quek, C.Y.J., Williamson, N.A., Mouradov, D., Sieber, O.M., Simpson, R.J., Salim, A., et al. (2015). FunRich: An open access standalone functional enrichment and interaction network analysis tool. Proteomics *15*, 2597–2601. https://doi.org/10.1002/pmic.201400515.
73. Andreozzi, P., Simó, C., Moretti, P., Porcel, J.M., Lüdtke, T.U., Ramirez, M.d.L.A., Tamberi, L., Marradi, M., Amenitsch, H., Llop, J., et al. (2021). Novel Core-Shell Polyamine Phosphate Nanoparticles Self-Assembled

from PEGylated Poly(allylamine hydrochloride) with Low Toxicity and Increased In Vivo Circulation Time. Small *17*, e2102211. https://doi.org/10.1002/smll.202102211.

74. Almeida, A., Delgado-Esteban, M., Bolaños, J.P., and Medina, J.M. (2002). Oxygen and glucose deprivation induces mitochondrial dysfunction and oxidative stress in neurones but not in astrocytes in primary culture. J. Neurochem. *81*, 207–217. https://doi.org/10.1046/j.1471-4159.2002.00827.x.
75. Rodriguez, C., Ramos-Araque, M.E., Dominguez-Martinez, M., Sobrino, T., Sanchez-Moran, I., Agulla, J., Delgado-Esteban, M., Gomez-Sanchez, J.C., Bolanos, J.P., Castillo, J., and Almeida, A. (2018). Single-Nucleotide Polymorphism 309T>G in the MDM2 Promoter Determines Functional Outcome After Stroke. Stroke *49*, 2437–2444. https://doi.org/10.1161/STROKEAHA.118.022529.
76. Lapresa, R., Agulla, J., Sanchez-Moran, I., Zamarreno, R., Prieto, E., Bolanos, J.P., and Almeida, A. (2019). Amyloid-ss promotes neurotoxicity by Cdk5-induced p53 stabilization. Neuropharmacology *146*, 19–27. https://doi.org/10.1016/j.neuropharm.2018.11.019.
77. Longhin, E.M., El Yamani, N., Rundén-Pran, E., and Dusinska, M. (2022). The alamar blue assay in the context of safety testing of nanomaterials. Front. Toxicol. *4*, 981701. https://doi.org/10.3389/ftox.2022.981701.
78. Koppula, P., Zhang, Y., Shi, J., Li, W., and Gan, B. (2017). The glutamate/cystine antiporter SLC7A11/xCT enhances cancer cell dependency on glucose by exporting glutamate. J. Biol. Chem. *292*, 14240–14249. https://doi.org/10.1074/jbc.M117.798405.
79. El Yamani, N., Collins, A.R., Rundén-Pran, E., Fjellsbø, L.M., Shaposhnikov, S., Zienolddiny, S., and Dusinska, M. (2017). In vitro genotoxicity testing of four reference metal nanomaterials, titanium dioxide, zinc oxide, cerium oxide and silver: towards reliable hazard assessment. Mutagenesis *32*, 117–126. https://doi.org/10.1093/mutage/gew060.
80. Collins, A., El Yamani, N., and Dusinska, M. (2017). Sensitive detection of DNA oxidation damage induced by nanomaterials. Free Radic. Biol. Med. *107*, 69–76. https://doi.org/10.1016/j.freeradbiomed.2017.02.001.
81. Dusinska, M., Mariussen, E., Rundén-Pran, E., Hudecova, A.M., Elje, E., Kazimirova, A., El Yamani, N., Dommershausen, N., Tharmann, J., Fieblinger, D., et al. (2019). In Vitro Approaches for Assessing the Genotoxicity of Nanomaterials. Methods Mol. Biol. *1894*, 83–122. https://doi.org/10.1007/978-1-4939-8916-4_6.
82. El Yamani, N., Rundén-Pran, E., Collins, A.R., Longhin, E.M., Elje, E., Hoet, P., Vinković Vrček, I., Doak, S.H., Fessard, V., and Dusinska, M. (2022). The miniaturized enzyme-modified comet assay for genotoxicity testing of nanomaterials. Front. Toxicol. *4*, 986318. https://doi.org/10.3389/ftox.2022.986318.
83. OECD (2016). Test No. 487: In Vitro Mammalian Cell Micronucleus Test (OECD Publishing).
84. Fenech, M. (2007). Cytokinesis-block micronucleus cytome assay. Nat. Protoc. *2*, 1084–1104. https://doi.org/10.1038/nprot.2007.77.
85. OECD (2016). Test No. 476: In Vitro Mammalian Cell Gene Mutation Tests using the Hprt and xprt genes. https://doi.org/10.1787/9789264264809-en.
86. El Yamani, N., Rubio, L., García-Rodríguez, A., Kažimírová, A., Rundén-Pran, E., Magdalena, B., Marcos, R., and Dusinska, M. (2022). Lack of mutagenicity of TiO(2) nanoparticles *in vitro* despite cellular and nuclear uptake. Mutat. Res. Genet. Toxicol. Environ. Mutagen. *882*, 503545. https://doi.org/10.1016/j.mrgentox.2022.503545.
87. Vasireddy, R.S., Sprung, C.N., Cempaka, N.L., Chao, M., and McKay, M.J. (2010). H2AX phosphorylation screen of cells from radiosensitive cancer patients reveals a novel DNA double-strand break repair cellular phenotype. Br. J. Cancer *102*, 1511–1518. https://doi.org/10.1038/sj.bjc.6605666.
88. Rodriguez-Gonzalez, R., Agulla, J., Perez-Mato, M., Sobrino, T., and Castillo, J. (2011). Neuroprotective effect of neuroserpin in rat primary cortical cultures after oxygen and glucose deprivation and tPA. Neurochem. Int. *58*, 337–343. https://doi.org/10.1016/j.neuint.2010.12.006.
89. Sun, X., Jung, J.H., Arvola, O., Santoso, M.R., Giffard, R.G., Yang, P.C., and Stary, C.M. (2019). Stem Cell-Derived Exosomes Protect Astrocyte Cultures From *in vitro* Ischemia and Decrease Injury as Post-stroke Intravenous Therapy. Front. Cell. Neurosci. *13*, 394. https://doi.org/10.3389/fncel.2019.00394.
90. Akkoc, Y., Dalci, K., Karakas, H.E., Erbil-Bilir, S., Yalav, O., Sakman, G., Celik, F., Arikan, S., Zeybek, U., Ergin, M., et al. (2023). Tumor-derived CTF1 (cardiotrophin 1) is a critical mediator of stroma-assisted and autophagy-dependent breast cancer cell migration, invasion and metastasis. Autophagy *19*, 306–323. https://doi.org/10.1080/15548627.2022.2090693.

STAR★METHODS

KEY RESOURCES TABLE

REAGENT or RESOURCE	SOURCE	IDENTIFIER
Antibodies		
Annexin V	Immunostep	#Ann V-DY634
Anti-MAP2 antibody	Invitrogen	#PA1-10005
Anti-mouse DyLight 549	Vector Laboratories	#DI-2549-1.5
Beta-III tubulin APC-conjugated antibody	R&D Systems	#IC1195A
Goat anti monkey IgG (H/L)	Bio-Rad	#AAI42
Neuron-specific beta-III tubulin APC-conjugated antibody ()	R&D Systems	#IC1195A
γ-H2AX primary antibody	Vell signaling	#9718
Chemicals, peptides, and recombinant proteins		
BD Via-Probe™ Cell Viability Solution	BD Biosciences	#555816
Enhanced chemiluminescence reagents	MIKX	Lot MK-S500
Evans blue dye	Sigma-Aldrich	#E2129
Proteomic columns	Eksigen, Dublin, CA, USA	Chrom XP C18 150 mm × 0.30 mm, 3 mm particle size, and 120 Å pore size
Medio Neurobasal™	Thermo Fisher Scientific	#21103049
rtPA	Alteplase, Activase®	Genentech, CA, USA
RIPA lysis buffer	Sigma-Aldrich	#20-188
Supplement B27	Thermo Fisher Scientific	#17504044
Triphenyltetrazolium chloride	Solarbio	Lot IT0160
Trifluoperazine	Solarbio	Lot 440-17-5
Triton X-100	Sigma-Aldrich	#9036-19-5
Critical commercial assays		
Amino acid precolumn derivatization kit	Waters	AccQ-Tag™
Colorimetric assay AlamarBlue (AB)	Thermo Fisher Scientific	#A50100
Fluorimetric caspase-3 assay kit	Sigma-Aldrich	#12161503
GOT Activity Assay Kit	Roche, Basel, Switzerland	# 10745120
GOT Activity Assay Kit	Abcam, Cambridge, UK	# ab263883
Glutamate assay kit	Abcam, Cambridge, UK	#ab138883
Mitochondrial membrane potential kit	Thermo Fisher Scientific	MitoProbe DilC1
Protein Assay Kit	Bio-Rad Laboratories, Hercules, CA, USA	RC DC™ Protein Assay Kit I 5000121
SensoLyte AMC tPA Activity Assay Kit	AnaSpec, Fremont, USA	# AS-72160
Experimental models: Cell lines		
C57BL/6J mouse: primary neuronal culture from mouse embryo (E14.5) cortices	CEBEGA (University of Santiago de Compostela)	N/A
C57BL/6J mouse: Primary cerebral cortical astrocyte from postnatal days 1–3 C57BL/6J	CEBEGA (University of Santiago de Compostela)	N/A
Mouse hippocampal HT-22	KERAFAST	#ESA111
Human neuroblastoma SH-5YSY	American Type Culture Collection (ATCC)	#CRL-2266
Human lymphoblastoid TK6	European Collection of Authenticated Cell Culture (ECACC)	N/A
Human astrocytes 1321N1	STAMI (collaborator)	N/A

(*Continued on next page*)

Continued

REAGENT or RESOURCE	SOURCE	IDENTIFIER
Experimental models: Organisms/strains		
Rat: Sprague-Dawley	CEBEGA (University of Santiago de Compostela)	N/A
Rat: Sprague-Dawley	Animal Facility Unit (CIC biomaGUNE)	N/A
Monkeys: *Macaca fascicularis*	Cynbiose (Institut Claude Bourgelat)	N/A
Software and algorithms		
BD CellQuest software,	Becton Dickinson Biosciences	https://www.bdbiosciences.com/
Biorender	Biorender	https://www.biorender.com/
FACSDiva software	BD Bioscience	https://www.bdbiosciences.com
FunRich	NA	http://funrich.org/index.html
GraphPad Prism software	Graphpad	https://www.graphpad.com/ (v.8.3.0)
ImageJ	NIH	https://imagej.nih.gov/ij/
Leica Application Suite Advance Fluorescence software	Leica	https://www.leica-microsystems.com
MarkerView software	SCIEX	https://sciex.com
MestReNova	Mestrelab	https://mestrelab.com/
Metafer	MetaSystems	https://metasystems-international.com/
MicroApp	NA	https://www.microapp.io (v. 2.0)
PeakView	SCIEX	https://sciex.com (v.2.2)
PMOD image analysis software	PMOD Technologies Ltd	https://www.pmod.comzen b (Version 3.5)
ProteinPilot software	SCIEX	https://sciex.com (v.5.0.1)
SPSS Statistics	IBM	https://www.ibm.com/ (v19.0)
ZEN blue software	ZEISS	https://www.zeiss.com (v. 2.3)
Other		
Rodent Anesthesia	Abbott	Sevoflurane
Serum tube sampling	Franklin Lakes	BD Microtainer K2E Tubes
tMCAo filament	Doccol	# 403512PK5Re
Laser Doppler	Perimed AB	Periflux 5000
Doppler probe	Perimed AB	Model 411
Grip strength device	Bioseb	# BIO-GS4
Rotarod apparatus	UgoBasile	# 47750-D01
Rectal temperature	Neos Biotec	N/A
Tube for venous blood collection	Smiths Medical	Polythene tube 800/100/200
Hybrid quadrupole-TOF mass spectrometer	SCIEX	QTOF6600+
Micro-LC system	Eksigen	Ekspert nLC425
Magnetic resonance imaging	Bruker	9.4 T horizontal bore magnet
PET-CT system	GE Healthcare	eXplore Vista-CT small animal
Biochemical analyzer (NHP samples)	Thermo Fisher Scientific	Konelab KL30 ISE
Confocal microscopy	Leica	DMI6000B
Flow cytometer analyser	BD Biosciences	BD FACSAria II
GABI radiometric detector	Elysia Raytest Gmbh	N/A
GOT activity analysis	Roche	Reflotron system
Hematology analyzer I (NHP samples)	Sysmex SAS	Sysmex XT-2000i
Hemostasis analyzer (NHP samples)	Diagnostica Stago SAS	Stago STart

(*Continued on next page*)

Continued

REAGENT or RESOURCE	SOURCE	IDENTIFIER
High-performance liquid chromatography (HPLC)	Agilent Technologies	1260 Infinity II
Plate fluorescence reader	Thermo Scientific	Fluoroskan Ascent FL
TissueLyser	Qiagen	TissueLyser II

EXPERIMENTAL MODEL AND STUDY PARTICIPANT DETAILS

Rodent care and housing

A total of 731 rats were included in this study (the total number of included and excluded animals per group is shown in Figure S15).

For rodent assays, protocols were approved by the Health Research Institute of Santiago de Compostela (IDIS) Animal Care Committee under procedure numbers 15011/2022/003 and 15010/2019/004, and the animal ethics committee of CIC biomaGUNE, in the case of PET analysis. The study was conducted according to the European Union (EU) guidelines (86/609/CEE, 2003/65/CE, and 2010/63/EU) and the ARRIVE guidelines. Male Sprague-Dawley rats (7–8 weeks old) weighing 250–300 g were used in this study. Animals were housed at an environmental temperature of 23°C with 40% relative humidity and were maintained on a 12 h light/dark cycle. Rats had *ad libitum* access to food and water. To minimize stress after arrival at the animal facility, the animals were allowed to acclimate to the facility for at least one week. Surgical procedures, PET and MR analysis were performed under sevoflurane anesthesia (6% induction and 4% maintenance with a mixture of 70% nitrous oxide and 30% oxygen). The rectal temperature was maintained at 37 $\pm$ 0.5°C using a feedback-controlled heating pad (Neos Biotec, Pamplona, Spain). The glucose levels analyzed before surgery were similar in the animals, ranging from 180 to 220 mg/dL. At the end of the procedure, rats were sacrificed under deep anesthesia (8% sevoflurane).

Experimental procedures in ischemic rodents were performed following five criteria derived from the Stroke Therapy Academic Industry Roundtable (STAIR) group guidelines for the preclinical evaluation of stroke therapeutics[57]: (1) cerebral blood flow was measured to confirm vascular occlusion as an index of the reliability of the ischemic model; (2) animals were randomly assigned to the treatment groups of the study; (3) researchers were blinded to treatment administration; (4) researchers were blinded to treatment during outcome assessment; and (5) temperature was controlled during the ischemic period.

Primate animal care and housing

A total 7 NHPs were included in this study (Figure S15). The protocol for the NHP experiments was reviewed by the Animal Welfare Body of Cynbiose and the Ethics Committee of VetAgro-Sup (Marcy l'Étoile, France) and approved under the number 1465-V2 (project number: 2016072117544328-v2). All experiments were conducted in accordance with European Directive 2010/63/UE, as published in the French Official Journal of February 7th, 2013. The animal facility was approved by the Association for Assessment and Accreditation of Laboratory Animal Care (AAALAC). Seven cynomolgus monkeys (*Macaca fascicularis,* males, average mean weight 3 kg) were included in the pharmacokinetic and safety studies. Animals were housed within the Cynbiose area (Institut Claude Bourgelat) under the following conditions: room temperature, 22°C; light cycle, 12 h light/dark cycle; and ventilation, at least 8 air changes per hour, with no air recirculation. Adequate amounts of a specific primate diet were provided daily according to the size and age of the animals (100 g for animals under 5 kg and 200 g for animals over 5 kg). The animals had *ad libitum* access to water. To minimize stress, the animals were allowed to acclimate to their designated housing rooms for two weeks. Blood sampling and treatment were performed on conscious and restrained animals. At the end of the *in vivo* experimental phase, each animal was kept in Cybiose and placed in a rest period.

Blood samples were collected by venipuncture of the femoral vessel into test tubes (BD Microtainer K2E Tubes, Franklin Lakes, New Jersey, USA). The tested treatment was administered *i.v.* at each dosing time point. The treatment solution (according to the dose required) was adjusted to inject approximately 1 mL in each animal, supplemented by 0.3 mL of injectable solution. For urine collection, animals were isolated overnight in individual modules, and diuretic trays were placed underneath the modules. The next day, urine was collected from the trays, filtered to remove as much feces and debris as possible, and aliquoted into 1 mL cryotubes.

Hematological, hemostasis, and biochemical parameters were analyzed using a hematology analyzer (Sysmex XT-2000i; Sysmex SAS, Kobe, Japan), Stago STart hemostasis analyzer (Diagnostica Stago SAS, Asniéres sur Seine, France), and Konelab KL30 ISE biochemical analyzer (Thermo Fisher Scientific, Massachusetts, USA), respectively, according to the specific analytical process of the device. Immunogenicity tests used to detect the presence of anti-GOT antibodies were performed using an ELISA sandwich with an anti-monkey IgG (H/L) HRP antibody (Bio-Rad, Hercules, CA, USA).

Surgical procedures in rats

Transient intraluminal middle cerebral artery occlusion (tMCAO) rat model: Transient focal ischemia (45 or 75 min, for mild and severe ischemia, respectively) was induced by intraluminal MCA occlusion as previously described[17,58] using commercially available sutures with silicone rubber-coated heads (350 μm in diameter and 1.5 mm long; Doccol, Sharon, MA, USA). Cerebral blood flow was monitored with a Periflux 5000 laser Doppler perfusion monitor (Perimed AB, Järfälla, Sweden) by placing the Doppler probe (model 411; Perimed AB) under the temporal muscle at the parietal bone surface near the sagittal crest. Once artery occlusion was achieved, as indicated by Doppler signal

reduction, each animal was carefully moved from the surgical bench to the MR system for baseline ischemic lesion assessment using MRI apparent diffusion coefficient (ADC) maps (before treatment administration). MR angiography (MRA) was also performed to ensure that the artery remained occluded throughout the procedure and to detect possible arterial malformations.[59] After basal MR analysis, the animals were returned to the surgical bench and the Doppler probe was repositioned. Reperfusion was performed 45 or 75 min after the onset of occlusion. In line with our previous study using the same ischemic model, the following exclusion criteria were used[58]: (1) <70% reduction in the relative cerebral blood flow during arterial occlusion, (2) arterial malformations, as determined by MRA, (3) baseline lesion volume <35% or >45% of the ipsilateral hemisphere, as measured using ADC maps, (4) absence of reperfusion or prolonged reperfusion (>10 min until achieving ≥50% of the baseline cerebral blood flow) after filament removal, and (5) failure to complete treatment. MRI-T2 scans for infarct assessment were performed at 1, 7, and 14 days after ischemia.

Embolic middle cerebral artery occlusion rat model (eMCAO): The embolic model was used according to a previously established protocol[24,60] with minimal modifications. Briefly, for clot preparation, venous blood was collected in a polythene tube (800/100/200; Smiths Medical, Minneapolis, MN, USA) from the tail vein of the donor rat. The tube containing blood was left to clot at 37°C for 2 h, and subsequently flushed out in a dish and rinsed with saline. The clot was cut to a length of 5 cm and drawn into a catheter. For ischemia induction, the common carotid, external carotid, and internal carotid arteries were carefully exposed after making a midline incision on the ventral side of the rat's neck. A clot-filled catheter tip was inserted through an incision into the internal carotid artery. The clot was infused using a syringe with a needle connected to the catheter at a rate of 10 μL of saline slowly over 1 min. As indicated for the tMCAO model, cerebral blood flow was monitored using laser Doppler flowmetry by placing the probe into a thinned skull in the MCA territory (4-mm lateral to bregma) to obtain a continuous measure of relative cerebral blood flow during the occlusion. MRI and ADC maps were obtained before treatment to confirm cerebral artery occlusion of the MCA. Follow-up MRI-T2 scans were performed on day 1 for lesion analysis. To induce reperfusion, rtPA (10 mg/kg; Alteplase, Activase; Genentech, CA, USA) was administered *i.v.* to the jugular vein (1 mL, 10% bolus, 90% perfusion for 30 min) 75 min after the clot occlusion. Effective arterial reperfusion was defined as when the blood flow recovered to at least 40% of the basal value determined at 30 min after treatment administration.

Treatment administration and collection of CSF or blood in rats: treatment administration was performed through the *i.v.* route through the tail vein, and each tested dose was adjusted to a final volume of 1 mL. CSF for GOT activity analysis was obtained from the cisterna magna and carried out using the protocol described elsewhere.[61] Briefly, using the occipital crest as a reference point, a midline incision was made beginning between the ears and ending approximately 2 cm caudally. The fascia was retracted and the muscles were dissected until the cisterna magna was exposed, which appeared as a tiny inverted triangle outlined by the cerebellum above and the medulla below, behind the translucent dural membrane. Once the cisterna magna was identified, a glass capillary was inserted, and 3–5 μL of CSF was collected at every puncture. CSF was collected, transferred to a tube, and kept frozen at −80°C until analysis. After 1 day of CSF sampling, the animals were sacrificed.

Blood samples for GOT and glutamate analyses were collected from the tail vein into test tubes (BD Microtainer K2E Tubes, Franklin Lakes, New Jersey, USA).

METHOD DETAILS

rGOT manufacturing and characterization

The human rGOT used in this study was produced and supplied by BiotechPharma UAB (Vilnius, Lithuania) using *E. coli* as host cells and SUMO technology to facilitate the expression and purification of the target protein with the Ala native N-terminus.[62,63] Enzymatic removal of the SUMO fusion junction and isolation of the protein from the host cells yielded a biologically active rGOT preparation with >95% purity. A description of the upstream biosynthesis and downstream purification processes as well as rGOT characterization by liquid chromatography with tandem mass spectrometry (LC-MS/MS) and matrix-assisted laser desorption/ionization-time of flight mass spectrometry (MALDI-TOF MS) are described in detail in the Patent Cooperation Treaty patent number WO2016157190A1.

MALDI-TOF MS (Figure S2A) revealed that, in accordance with the human form (EC 2.6.1.1), rGOT was a homodimeric polypeptide (92 kDa) consisting of two identical monomers (46 kDa). Moreover, results from tryptic digestion followed by liquid chromatography with tandem mass spectrometry identification using a human specific database (UniProt) revealed that identification of rGOT had <1% false discovery rate. As shown in Figures S2B and S2C, more than 1,300 peptides were identified with more than 91% GOT sequence coverage, which demonstrates the unambiguous identification of this protein in the native human GOT.

For LC-MS/MS characterization, 50 μL of trifluoroethanol (TFE, Sigma-Aldrich, Missouri, USA) was added to 50 μL rGOT and vortexed to yield a final concentration of 50% TFE. The protein was then reduced with 150 mM 1,4-dithiothreitol (Merck, Darmstadt, Germany) for 45 min at 55°C and carbamide methylated with 550 mM iodoacetamide (Merck, Darmstadt, Germany) for 30 min at room temperature in the dark. Samples were diluted with 50 mM Tris (2-amino-2-(hydroxymethyl)-1,3-propanediol (Sigma-Aldrich, Missouri, USA) at a pH of 8 to yield a 5% TFE solution. Trypsin (Promega, Madison, WI, USA) was added to a final ratio relative to rGOT of 1:25–1:50 (2 μg trypsin for 1–2 mg/mL rGOT) overnight at 37°C. Formic acid (FA, Sigma-Aldrich, Missouri, USA) was added to stop the reaction, and the digested peptides were purified using C18 Spin Tips (Thermo Scientific Pierce, Massachusetts, USA) following the manufacturer's instructions. Finally, the sample was diluted in water and 0.1% FA and analyzed by LC-MS/MS, as described in the library creation (data-dependent acquisition [DDA] method), using a 90 min gradient. For MALDI-TOF MS characterization, the protein was dissolved in 125 mL of MeOH/H_2O with 1% of trifluoroacetic acid (TFA, Scharlau, Barcelona, Spain). One microliter was mixed with 20 μL (1:20 dilution) of sinapinic acid (Sigma-Aldrich, Missouri, USA) solution (20 mg/mL Sa dissolved in 100% MeOH; Scharlau, Barcelona, Spain) and analyzed by MALDI-TOF. One microliter aliquots were deposited

onto a 384 384 Opti-TOF MALDI plate (Applied Biosystems, Foster City, CA, USA). MALDI analysis was performed on a 4800 MALDI-TOF/TOF analyzer (Applied Biosystems, Foster City, CA, USA).

Mass spectrometry (MS) spectra were acquired in reflector positive-ion mode using an Neodymium-doped Yttrium Aluminum Garnet (Nd:YAG)laser with a wavelength of 355 nm and an average of 100 laser shots. The mass of the compound protein was determined by an external calibration approach using protein standard calibration I (Bruker-Daltonics, MA, USA). Insulin (m/z = 5734.51), ubiquitin I (m/z = 8565.76), cytochrome *c* (m/z = 12360.97), and myoglobin (m/z = 16952.30) were used as internal standards. Stability studies of rGOT revealed that it retained its original activity (U/mg enzyme) when kept frozen at −20°C.

The synthesis and characterization of rGOT-PEG were performed as previously described.[21]

tPA activity analysis

tPA activity was analyzed using the SensoLyte AMC tPA Activity Assay Kit (AnaSpec, Fremont, USA), according to the manufacturer's specifications. Leupeptin was used as the control inhibitor of tPA.

GOT activity analysis

GOT activity in the blood was measured using the Reflotron system (Roche, Basel, Switzerland) using specific GOT/AST activity test strips. GOT activity in the CSF was determined using an aspartate aminotransferase activity assay kit (Abcam, Cambridge, UK) following the manufacturer's recommended protocol.

Blood glutamate analysis

The concentration of glutamate in the blood was determined by two methods: high-performance liquid chromatography (HPLC) (1260 Infinity II; Agilent Technologies, Santa Clara, CA, USA) using the AccQ-Tag precolumn derivatization method for amino acid analysis (Waters, Milford, MA, USA) and a glutamate assay kit (Abcam, Cambridge, UK) following the manufacturer's recommended protocol.

Magnetic resonance imaging and image analysis

MRI studies were conducted with a 9.4 T horizontal bore magnet (Bruker BioSpin, Ettlingen, Germany) with 12-cm wide actively shielded gradient coils (440 mT/m). Radiofrequency transmission was achieved using a birdcage volume resonator, and the signal was detected using a four-element arrayed surface coil positioned over the head of the animal. The latter was fixed using a tooth bar, earplugs, and adhesive tape. The transmission and reception coils are actively decoupled from each other. Gradient–echo pilot scans were performed at the beginning of each imaging session to accurately position the animal inside the magnet bore. MRI post-processing was performed using the ImageJ software (https://imagej.nih.gov/ij/). Infarct volumes were determined from ADC maps and T2 relaxation maps by manually selecting areas with reduced ADC values or hyperintense T2 signals by a researcher blinded to the animal protocols. Infarct size was defined as the percentage of ischemic damage with respect to the ipsilateral hemispheric volume, corrected for brain edema. For each brain slice, the total area of both hemispheres and areas of infarction were calculated. The edema index was measured by quantifying the midline deviation (MD), which was calculated as the ratio between the volume of the ipsilateral hemisphere and the volume of the contralateral hemisphere. The actual infarct size was adjusted for edema by dividing the infarction area by the edema index [mm^3/MD]. Thereafter, infarct volume was calculated as follows: (infarct volume [mm^3/MD]/ipsilateral hemispheric area [mm^3]) × 100. These procedures have been repeatedly used in the literature to measure and evaluate stroke outcomes in experimental models.[17,18,21]

ADC maps

ADC maps were acquired during MCA occlusion (approximately 30 min after the onset of ischemia) using a spin-echo echo-planar imaging sequence with the following acquisition parameters: echo time (ET) = 26.91 ms, repetition time (RT) = 4 s, spectral bandwidth (SW) = 200 kHz, 7 b-values of 0, 300, 600, 900, 1200, 1600, and 2000 s/mm^2; flip angle (FA) = 90°; number of averages (NA) = 4; 14 consecutive slices of 1 mm, 24 × 16 mm^2 field-of-view (FOV) (with saturation bands to suppress signal outside this FOV), a matrix size of 96 × 64 (isotropic in-plane resolution of 250 μm/pixel × 250 μm/pixel), and implemented with the fat suppression option. Based on previous studies,[18,21,58] the ADC values in the healthy rat brain normally do not fall below 0.55 × 10^{-3} mm^2/s; therefore, this threshold provides a convenient means of segmenting abnormal tissue.

MR angiography

Non-invasive angiography was evaluated with time-of-flight magnetic resonance angiography (TOF-MRA) as reported previously.[58,59] TOF-MRA scans were performed with a 3D-Flash sequence with an ET = 2.5 ms, RT = 15 ms, FA = 20°, NA = 2, SW = 98 kHz, 1 slice of 14 mm, 30.72 × 30.72 × 14 mm^3 FOV (with saturation bands to suppress signals outside this FOV), a matrix size of 256 × 256 × 58 (resolution of 120 μm/pixel × 120 μm/pixel × 241 μm/pixel), and implemented without the fat suppression option.

MRI T2-maps

Ischemic lesions were determined from T2-maps calculated from T2-weighted imagesacquired 24 h, 7, and 14 days after the onset of ischemia using an multi-slice-multi-echo sequence: ET = 9 ms, RT = 3 s, 16 echoes with 9 ms echo spacing, flip angle = 180°, NA = 2, SW = 75 kHz,

14 slices of 1 mm, 19.2 × 19.2 mm^2 FOV (with saturation bands to suppress signals outside this FOV), a matrix size of 192 × 192 (isotropic in-plane resolution of 100 μm/pixel ×100 μm/pixel), and implemented without the fat suppression option.

MR spectroscopy

Spectroscopic analysis of metabolites (glutamate, aspartate, and lactate) in the brain was performed as previously described.[18] Local shimming was performed by manually adjusting the first- and second-order shim coil currents using a proton-stimulated echo acquisition mode (STEAM)-waterline sequence. The field homogeneity in a 3 × 3 × 3 mm^3 voxel typically resulted in signal linewidths of 10–20 Hz for the water signal. *In vivo* ^{1}H magnetic resonance spectra of both hemispheres of the rat brain were acquired using an STEAM-^{1} H sequence with an ET = 3 ms, mixing time = 10 ms, RT = 1500 ms, FA = 90°, NA = 200, cubic voxel = 3 × 3 × 3 mm^3, and acquisition time = 5:15 min. The water signal was suppressed using variable-power radio frequency pulses with optimized relaxation delays. Spectra were processed using MestReNova software (Mestrelab Research, Santiago de Compostela, Spain). For quantitative analysis, the glutamate, aspartate, and lactate signals were normalized to the creatine peak/phosphocreatine areas for each spectrum. MRS was performed during occlusion and after reperfusion (30, 60, 90, and 120 min after reperfusion).

Quantitative proteomic analysis using the SWATH approach in brain tissue

Perfusion and tissue processing

Animals were deeply anesthetized with sevoflurane (6% in a mixture of 70% NO_2 and 30% O_2) and transcardially perfused with 100 mL of 0.1 M PBS (pH 7.4). Brains were carefully removed from the skull and sectioned (2-mm thick) using a matrix. Tissues were stored at 80°C until further analysis.

Protein extraction and digestion

Frozen tissue (100 mg) from the different brain samples was [SBl1] homogenized in RIPA buffer (200 mM Tris/HCl [pH 7.4], 130 mmol/L NaCl, 10% [v/v] glycerol, 0.1% [v/v] SDS, 1% [v/v] Triton X-100, and 10 mmol/L $MgCl_2$) with anti-proteases and anti-phosphatases (Sigma-Aldrich, St. Louis, MO, USA) in a TissueLyser II (Qiagen, Tokyo, Japan). The homogenate was centrifuged at 14,000 × *g* at 4°C for 20 min. The protein concentration was measured using an RC-DC kit (Bio-Rad Laboratories, Hercules, CA, USA) according to the manufacturer's protocol. Protein aliquots of 100 μg were concentrated in an SDS-PAGE single band[64,65] and subjected to manual digestion, as described elsewhere.[66] Finally, the peptides were dissolved in 0.1% FA for further analysis.

Quantitative SWATH analysis

Quantitative proteomic analysis was performed using the SWATH method with a hybrid quadrupole-TOF mass spectrometer, 6600+ (SCIEX, Framingham, MA, USA), as described previously by our group.[67–69]

Generation of the reference spectral library

A pool of each group was analyzed using a shotgun DDA approach. The samples were separated in a micro-LC system Ekspert nLC425 (Eksigen, Dublin, CA, USA) using a Chrom XP C18 150 mm × 0.30 mm, 3 mm particle size, and 120 Å pore size (Eksigen, Dublin, CA, USA) at a flow rate of 10 μL/min, using solvent A water, 0.1% FA and solvent B acetonitrile, 0.1% FA. The peptide separation gradient ranged from 5% to 95% B for 30 min, 5 min at 90% B, and, finally, another 5 min at 5% B for column equilibration, for a total time of 40 min. The LC was coupled with a hybrid quadrupole-TOF mass spectrometer (6600+; SCIEX, Framingham, MA, USA). Using the mass spectrometer, a 250 ms survey scan was performed from 400 to 1250 m/z, followed by MS/MS experiments from 100 to 1500 m/z (acquisition time of 25 ms) for a total cycle time of 2.8 s. The fragmented precursors were added to the dynamic exclusion list for 15 s, and any ion with a charge of +1 was excluded from MS/MS analysis. Protein identification was performed using ProteinPilot software v.5.0.1. (SCIEX, Framingham, MA, USA) using a *Rattus norvegicus* or human (to detect human rGOT administered to the rats)-specific UniProt Swiss-Prot database. The false discovery rate was set to 1 for peptides and proteins, with a confidence score above 99%.[70]

Quantification by SWATH and data analysis

SWATH–MS acquisition was performed using an independent data analysis method. Four micrograms of protein from each sample were subjected to chromatographic separation, as described previously.[68] The SWATH method consisted of repeating a cycle consisting of the acquisition of 100 TOF MS/MS scans (400–1500 m/z, high sensitivity mode, 50 ms acquisition time) of overlapping sequential precursor isolation windows of variable width (1 m/z overlap) covering the 400–1250 m/z mass range with a previous TOF MS scan (400–1500 m/z, 50 ms acquisition time) for each cycle. The total cycle time was 6.3 s. For each sample set, the width of the 100 variable windows was optimized according to the ion density found in the DDA runs using the SWATH variable window calculator worksheet from Sciex.[68]

The targeted data extraction of the fragment ion chromatogram traces from the SWATH runs was performed using PeakView (version 2.2) and the SWATH Acquisition MicroApp (version 2.0). This application processed the data using the spectral library created from the DDA data loading over this library of individual samples acquired using the SWATH method. To obtain peak areas of up to 10 peptides per protein, seven fragments per peptide were selected based on the signal intensity; any shared and modified peptides were excluded from processing.

The integrated peak areas (SWATH areas) were directly exported to the MarkerView software (AB SCIEX) for relative quantitative analysis. MarkerView uses processing algorithms that accurately find chromatographic and spectral peaks directly from the raw SWATH data. First, the integrated peak areas were normalized using multiple linear regression normalization or sum total areas, depending on which analysis was performed, and unsupervised multivariate statistical analysis using principal component analysis was performed to compare the data across the samples, using scaling. Student's t test analysis using the MarkerView software was performed to compare the samples. The deregulated proteins were selected using a *p*-value <0.05 and *FC > 1.5 or < 0.8* as cut-off values. The individual values of SWATH areas per protein and sample were used to create box pots.

Protein functional enrichment and network analysis: The differentially regulated proteins were subjected to functional analysis and interpreted through various open access bioinformatics tools for analyzing biological information related to molecular functions, biological processes, cellular components, protein classes, pathways, and networks among large and complex datasets. FunRich (http://funrich.org/index.html) was used for functional enrichment and interaction network analysis. FunRich uses hypergeometric tests, Benjamini–Hochberg procedure[71] and Bonferroni method.[72]

Radiolabeling

Synthesis of [^{18}F]F-PyTFP

[^{18}F]F-PyTFP was synthesized using a TRACERlab FX-FN synthesis module (GE Healthcare, Waukesha, WI, USA), following a previously described procedure.[73] Briefly, aqueous [^{18}F]fluoride was first trapped in an ion-exchange resin (Sep-Pak Accell Plus QMA Light; Waters, Milford, MA, USA) and subsequently eluted into the reactor vessel using a solution of Kryptofix $K_{2.2.2}$/K_2CO_3 in a mixture of water and acetonitrile. After azeotropic drying of the solvent, a solution of F-PyTFP (10 mg) in a mixture of *tert*-butanol and acetonitrile (4:1) was added, and heated at 40°C for 15 min. The reaction mixture was then diluted with 1 mL each of acetonitrile and water, and purified by HPLC using a Nucleosil 100-7 C18 column (Machery-Nagel, Düren, Germany) as the stationary phase and 0.1% TFA/acetonitrile (25:75) as the mobile phase at a flow rate of 3 mL/min. The desired fraction (retention time = 22–23 min; [^{18}F]F-PyTFP) was collected, diluted with ultrapure water (25 mL), and flushed through a C18 cartridge (Sep-Pak Light, Waters, Milford, MA, USA) to selectively retain [^{18}F]F-PyTFP. The desired labeled fraction was finally eluted using acetonitrile (1 mL). Radiochemical purity was determined by radio-HPLC, using an Agilent 1200 Series chromatograph equipped with a multiple wavelength ultraviolet (UV) detector (λ = 254 nm) and a GABI radiometric detector (Elysia Raytest Gmbh, Radeberg, Germany) connected in series. A Mediterranean C18 column (4.6 × 150 mm, 5 μm) was used as the stationary phase and 0.1% TFA/acetonitrile (0–1 min of 25% acetonitrile; 1–9 min of 25–90% acetonitrile; 9–12 min of 90% acetonitrile; 12–13 min of 90–25% acetonitrile; 13–15 min of 25% acetonitrile) as the mobile phase at a flow rate of 1.5 mL/min (retention time = 7.5 min).

Radiolabeling of rGOT with ^{18}F

The radiofluorination of rGOT protein with ^{18}F was carried out by the reaction between the free amine groups of lysine residues present in the protein and [^{18}F]F-PyTFP. Briefly, 30 μL of GOT solution (6.86 mg/mL) was diluted in 100 μL of saline solution (0.9% NaCl), and mixed with 10 μL of [^{18}F]F-PyTFP in acetonitrile (approximately 232 ± 71 MBq). The reaction mixture was incubated at 40°C for 30 min. After incubation, the crude reaction mixture was purified by size exclusion chromatography using Nap-5 Sephadex G-25 DNA grade columns (GE Healthcare, Waukesha, WI, USA) preconditioned with saline solution (0.9% NaCl). The fractions containing pure labeled compound were collected, the amount of radioactivity was measured in a dose calibrator (CPCRC-25R; Capintec Inc., NJ, USA), and analyzed by radio-HPLC, using an Agilent 1200 Series chromatograph equipped with a multiple wavelength UV detector (λ = 254 nm) and a GABI radiometric detector (Elysia Raytest Gmbh, Radeberg, Germany) connected in series. A Mediterranean C18 column (4.6 × 150 mm, 5 μm) was used as the stationary phase and 0.1% TFA water/acetonitrile (0–1 min of 25% acetonitrile; 1–9 min of 25–90% acetonitrile; 9–12 min of 90% acetonitrile; 12–13 min of 90–25% acetonitrile; 13–15 min of 25% acetonitrile) as the mobile phase at a flow rate of 1.5 mL/min (retention time = 5.2 ± 0.2 min).

PET imaging studies

Rats were anesthetized by inhalation of 5% isoflurane (IsoFlo, Abbott Laboratories, Illinois, USA) in pure O_2 and maintained using 1.5–2% isoflurane in 100% O_2. During imaging, rats were kept normothermic using a heating blanket (Homeothermic Blanket Control Unit; Bruker). Once the animal was under anesthesia, one of the lateral tail veins was catheterized using a 24-gauge catheter (Introcan Certo; B. Braun), and [^{18}F]rGOT was injected using saline solution as the vehicle (195 ± 90 MBq for control animals; 180 ± 95 for ischemic animals; dose adjusted to 1 mg/kg) concomitantly with the start of PET dynamic acquisition. Dynamic PET images (frames: 4 × 30 s, 4 × 45 s, 4 × 120 s, 4 × 240 s, 4 × 480 s, 3 × 1200 s; total duration = 121 min) were acquired using an eXplore Vista-CT small animal PET-CT system (GE Healthcare, WI, USA) in four bed positions to cover the entire animal. Computed tomography (CT) scans were acquired immediately after each PET acquisition. PET images were reconstructed with Filtered Back Projection using random, scatter, and attenuation correction and a ramp filter with a cutoff frequency of 1 Hz. Images were analyzed using π- PMOD image analysis software (Version 3.5, PMOD Technologies Ltd, Zurich, Switzerland). For cerebral and whole-body distribution, volumes of interest were manually drawn in whole brain, kidneys, liver, bladder, and heart using the CT images for anatomical reference, and decay-corrected time–activity curves were obtained.

CellPress
OPEN ACCESS

Motor and somatosensory tests

Sensorimotor deficits were evaluated using the cylinder test, grip strength test, and rotarod test, as reported elsewhere.[21] All tests were performed during the dark cycle of animal housing, with environmental conditions consistently maintained across examinations, and by a researcher blinded to the animal grouping. These tests were performed 1 day before surgery and 7 and 14 days after ischemia induction. A baseline functional evaluation was required to test for preoperative bias.

Cylinder test

Somatosensory deficits were evaluated by examining limb asymmetry during exploratory activity. For this test, animals were introduced into a plexiglas cylinder (diameter 20 cm; height 40 cm), and a video camera, located under this transparent cylinder, was used to record the vertical exploratory movement of the animal's forelimbs for 5 min. The laterality index was calculated as the number of times the animal touched the cylinder with the impaired forelimb during the ascendant movement divided by the number of total touches (impaired and non-impaired forelimb contacts). This index is close to 0.5 for healthy animals, and tends to be 0 or 1 for animals that preferentially use the right or left paw, respectively.

Grip strength test

This test was used to assess motor function and deficits and was performed using a grip strength device (Bioseb, Pinellas Park, USA). The animal's paws were placed on a grid to which the animal was held, while its tail was gently pulled backward. The maximum grip strength prior to grip release was recorded. Multiple test sessions were conducted, with each session consisting of three trials. The average of the three trials was considered the average performance.

The rotarod test was performed using a rotarod apparatus (UgoBasile, Comerio, Italy) to evaluate motor balance and coordination impairments. Before surgery, the animals were pre-trained for 3 consecutive days (each animal received three training sessions per day). Rats were placed on the rotarod at a constant speed of 20 rpm. The time that the animal could stay on the rotarod was measured with 120 s as the cut-off limit.

Apoptosis analysis of rGOT treatment in primary cortical neurons subjected to ischemic model of oxygen-glucose deprivation (OGD)

Neuronal protection mediated by apoptosis cell death was developed in primary neuronal culture. Primary neuronal cultures were prepared from C57BL/6J (The Jackson Laboratories) mouse embryo (E14.5) cortices. Animals were maintained in specific-pathogen free facilities at the University of Salamanca, in accordance with Spanish legislation (RD53/2013) under license from the Spanish government and the European Union (2010/63/EU). Protocols were approved by the Bioethics Committee of the Institute of Biomedical Research of Salamanca. All efforts were made to minimize the number of animals used and ensure minimal suffering. Neurons were seeded at 1.8 x 10^5 cells/cm^2 in Neurobasal medium (Invitrogen), supplemented with 2% B27 (Invitrogen) and 2 mM glutamine (Invitrogen), and incubated at 37°C in a humidified 5% CO_2-containing atmosphere. Culture medium was replaced with fresh medium every 3 days. Neurons were used for the experiments on day 8–9 *in vitro*.[31] All experiments were replicated in the number (3–4) of neuronal cultures indicated in the figure legends, which were performed from different pregnant females.

Protection analysis was developed in primary cortical neurons subjected to ischemic model of oxygen-glucose deprivation (OGD). After 8–9 days in culture, neurons were subjected to OGD by incubating neurons at 37°C in an incubator equipped with an air lock and continuously gassed with 95% N_2/5% CO_2, for 90 min. The incubation medium (Neurobasal without glucose) was previously gassed with 95% N_2/5% CO_2, for 5 min. In parallel, neurons were incubated in Neurobasal medium (normoxia) at 37°C, in a humidified atmosphere of 95% air/5% CO_2.[74] After OGD, neurons were further incubated in Neurobasal medium at 37°C, in a humidified atmosphere of 95% air/5% CO_2 (reoxygenation),[75] in the absence or presence of increasing concentrations of recombinant GOT (1.8, 3.7, 15, 30 or 50 μg/mL), for 24 h.

Apoptosis cell death was determined by Active caspase-3 determination, flow cytometry detection of neuronal apoptosis and mitochondrial membrane potential. For active caspase-3 analysis, fluorimetric caspase-3 assay kit (Sigma) was used, following the manufacture's protocol. Briefly, neurons were lysed with 50 mM HEPES, 5 mM CHAPS, 5 mM DTT, pH 7.4 for 20 min on ice, and the assay buffer containing the Ac-DEVD-AMC (acetyl-Asp-Glu-Val-Asp-7-amino-4-methylcoumarin) substrate (20 mM HEPES, 2 mM EDTA, 0.1% CHAPS, 5 mM DTT, 16 μM Ac-DEVD-AMC, pH 7.4) was added. Aliquots of 200 μL were transferred to a 96-wells plate and the fluorescence was recorded at 5 min intervals for 30 min at 37°C using a Fluoroskan Ascent FL (Thermo Scientific) fluorimeter (excitation: 360 nm, emission: 460 nm). Caspase-3 activity was determined as 7-amino-4-methylcoumarin (AMC) release rate extrapolating the slopes to those obtained from the AMC standard curve. Results were expressed as pmol/h/μg protein.[31]

In case of flow cytometry detection, neurons were carefully detached using 1 mM EDTA tetrasodium salt in phosphate-buffered saline (PBS, 136 mM NaCl, 2.7 mM KCl, 7.8 mM $Na_2HPO_4 \cdot 2H_2O$, 1.7 mM KH_2PO_4, pH 7.4) at room temperature. Neurons were stained with annexin V-DY634 (AnnV; Immunostep) and 7-aminoactinomycin D (7-AAD; Becton Dickinson Biosciences) in binding buffer (100 mM HEPES, 140 mM NaCl, 2.5 mM $CaCl_2$) to quantitatively determine the apoptosis by flow cytometry. Annexin V-positive neurons that were 7-AAD-negative were considered apoptotic. The mitochondrial membrane potential ($\Delta\psi_m$) was assessed using the MitoProbe $DiIC_1$ (1,1′, 3, 3, 3′, 3′-hexamethylindodicarbo-cyanine iodide) assay kit for flow cytometry (Life Technologies), following manufacturer's instructions. Neurons were incubated with the dye at 37 °C for 30 min. $\Delta\psi_m$ values were expressed as percentages, using carbonyl cyanide 4-(trifluoromethoxy) phenylhydrazone

(CCCP; 10 μM) for 15 min to define the 0% $\Delta\psi_m$ value. Triplicates obtained from four different cultures were analyzed on a FACScalibur flow cytometer (15 mW argon ion laser tuned at 488 nm; BD CellQuest software, Becton Dickinson Biosciences).[76]

Cell protection analysis of rGOT treatment in cell lines submitted to OGD and glutamate excitotoxicity

Cell protection analysis was developed in mouse hippocampal HT-22 and human neuroblastoma SH-5YSY cell lines. Mouse hippocampal HT-22 cell line was purchased from KERAFAST. These cells were cultured in high glucose DMEM medium supplemented with 10% Fetal bovine serum (FBS),1% penicillin/streptomycin and 1mM sodium pyruvate. Human neuroblastoma SH-5YSY cells were purchased from the American Type Culture Collection (ATCC) and cultured in DMEM/F-12 medium supplemented with 10% FBS and 1% penicillin/streptomycin.

For glutamate excitotoxicity, the HT-22 and SH-5YSY cells were seeded in 96 well plate (15000 cells/well) 24 h before exposure. Glutamate excitotoxicity was induced by incubating HT-22 and SH-5YSY cells to 20 mM glutamate for 5 and 6 h respectively. After completion of glutamate excitotoxicity, cells were replenished with fresh culture media added with 10 μg/ml rGOT particles, and exposed for 24 h to investigate potential neuroprotective effect. Cell viability was measured by the AB assay as described.[77] Ischemia was induced *in vitro* by OGD 24 h post-seeding by culturing HT-22 and SH-5YSY cells in glucose-depleted medium and in a hypoxic environment (1% oxygen) for 5 h. After OGD, the cells were moved to cell culture medium containing 10 μg/ml rGOT particles and cultured under normoxic conditions to mimic reperfusion. The cytotoxicity in response to glutamate (Merck PHR2634-1G) excitotoxicity and oxygen- and glucose deprivation (OGD) was measured by the colorimetric assay AlamarBlue (AB) (Fisher Scientific).

After glutamate exposure and OGD treatment, 5 μL of media was collected in 96-well plate, mixed with 95 μL of cold PBS, and stored at −20°C. The Glutamate-Glo assay (Promega, J7021) was used to measure glutamate levels. The principle of this assay is that Glutamate dehydrogenase uses the glutamate present in the media in presence of NAD^+ to produce αKG and NADH. In the presence of NADH, a pro-luciferin reductase substrate is converted to luciferin, which is then used by Ultra-Glo recombinant luciferase to produce light. The luminescent signal was subsequently measured by an OPTIMA microplate reader (BMG Labtech). All values were normalized to negative control (complete medium).[78]

In vitro cytotoxic and genotoxic analysis of rGOT

Dose response toxicity analysis of rGOT was tested on different cell lines and by testing cytotoxicity, DNA damage, chromosomal damage and gene mutation. Tox analysis was performed in mouse hippocampal HT-22, human neuroblastoma SH-5YSY cell lines, human astrocytes 1321N1, human lymphoblastoid TK6 cells and Chinese hamster lung fibroblast V79-4 cells.

Mouse hippocampal HT-22 and human neuroblastoma SH-5YSY cell lines. Mouse hippocampal HT-22 cell line was purchased from KERAFAST. These cells were cultured in high glucose DMEM medium supplemented with 10% Fetal bovine serum (FBS),1% penicillin/streptomycin and 1mM sodium pyruvate. Human neuroblastoma SH-5YSY cells were purchased from the American Type Culture Collection (ATCC) and cultured in DMEM/F-12 medium supplemented with 10% FBS and 1% penicillin/streptomycin. Human astrocytes 1321N1 cell line was a gift from our collaborator (STAMI). The astrocytes were maintained in high glucose DMEM medium supplemented with 10% FBS and 1% penicillin/streptomycin. The human lymphoblastoid TK6 cells were purchased from the European Collection of Authenticated Cell Culture (ECACC) and cultured in RPMI medium with 9% horse serum and 1% penicillin/streptomycin. The Chinese hamster lung fibroblast V79-4 cells were purchased from ECACC and cultured in low glucose DMEM supplemented with 10% Fetal bovine serum (FBS),1% penicillin/streptomycin and 2mM glutamine. All cells were maintained in an incubator at 37°C, 5% CO_2.

Cytotoxicity was tested using the AlamarBlue (AB) assay

The AB assay assesses cell viability by the metabolic activity of living cells through conversion of resazurin compound (oxidised form) to resorufin (reduced form).[77] The HT-22, SH-5YSY, 1321N1and TK6 cells were seeded in 96 well plate (15000 cells/well) 24 h (h) before exposure. The day of exposure, cells were exposed to a range of rGOT concentrations (0,1 to 30 μg/mL) in duplicate wells for 3 or 24 h. At the end of exposure, we followed the test as described by.[77,79] As positive control, the chlorpromazine hydrocholoride (CHL, 50 μM) was used. In addition, untreated cells (cells in culture medium) were used as negative control and cells incubated with MilliQ water at the highest concentration of rGOT tested used as solvent control. Three independent experiments were performed for each cell line except for astrocytes cells where only two independent experiments were conducted.

DNA damage by the enzyme-linked version of the comet assay

The miniaturized enzyme-linked version of the comet assay is a widely used method for detection of DNA damage in cells with nuclei. It detects both DNA strand breaks and specific DNA lesions, such as oxidized purine, which can be detected by treating the cells with specific enzymes, such as formamidopyrimidine DNA glycosylase (Fpg), which recognize oxidized purines.[80,81] The assay was performed as described[82] on HT-22, SH-5YSY, 1321N1 and TK6 cells. Briefly, cells were seeded in 96 well plate (15000 cells/well) for 24 h before exposure. The cells were exposed to a range of rGOT concentration (0,1–30 μg/mL). At the end of exposure, the cells were washed with PBS, trypsinized (in case of adherent cells) and resuspended in 200 μL of cell culture media. Cells were then mixed with 0.8% low melting agarose at 37°C and gel drops put on glass slides pre-coated with 0.5% normal melting agarose before proceeding with electrophoresis until DNA visualization and analysis.[82] In total, three independent experiments were performed for each cell line except for 1321N1 cells where only two independent

experiments were conducted. All experiments included positive controls (100 μM H_2O_2 and 0.2 mM MMS) for 3 and 24 h and negative control (untreated cells in cell culture medium).

Chromosomal damage by the cytokinesis block micronucleus (CBMN) assay

The *in vitro* cytokinesis-blocked micronucleus (CBMN) assay is the gold-standard to investigate genotoxicity by chromosomal damage in a broad range of cell lines. The CBMN assay can be used to detect both clastogenic or aneugenic DNA damage, chromosomal breakage or the loss or gain of an entire chromosome. The assay detects micronucleus (Mn) in the cytoplasm of interphase cells. The Mn is formed from chromosome or chromatid fragments that lag in mitotic cell division. These fragments can be stained and visualized.[81] To detect MN in response to test particles, CBMN assay was performed o on TK6 cell lines.

The TK6 cells (1x10^6 cells/ml) were exposed to rGOT (0.1–15 μg/mL) for 24 h. At the end of the exposure, the cells were washed in PBS and cytochalasin B (CytB, 0.3 μg/mL) was added and cells incubated for 1.5–2 cycles to stop cytokinesis and for expression of DNA damage. After the expression period, the cells were washed with PBS, mixed 1:1 with hypotonic KCl (0.075M) and gently mixed by inversion. For cell fixation, an aliquot of one-tenth volume of cold fixative (methanol/glacial acetic acid 3:1) was added and gently mixed. Cells are harvested by centrifugation (200 × g for 5 min) and the supernatant is aspirated. An aliquot of additional fixative was added equal to the original cell volume removed from the culture. For slide preparation, cytospin centrifuge (Bergman) to drop cells (about 1000 cells/drop) directly into clean microscopic slides was used. Each drop on slides were then stained using 4′,6′-diamino-2phenyl-indole (DAPI) in vectashield, 1 μg/mL. For cytotoxicity evaluation, at least 1000 cells (500 cells per replicate culture) were evaluated to determine the Cyt B proliferation index (CBPI) at each dose level and controls and CBPI calculated as described in OECD test guidelines 487.[83] For genotoxicity (Mn% per binucleated BN cells), at least 1000 (BN) cells per replicate were scored for the presence of MN per concentration following criteria.[84] For both cytotoxicity and genotoxicity, an automatic scoring system with Metafer software (Metasystems Germany) was used. In total two independent experiments were performed each including 2 replicates. Every experiment included negative (untreated cells in culture media) and positive control (Mitomycin MMC, 0.5 μg/mL).

$$CBPI = \left(\frac{(1 \times Mononucleated\ cells)+(2 \times Binucleated\ cells)+(3 \times Multinucleated\ cells}{Total\ number\ of\ cells\ scored} \right)$$

Gene mutation detection using HPRT (hypoxanthine phosphoribosyl-transferase) mammalian gene mutation assay

The mammalian *in vitro* HPRT gene mutation test was used following the OECD test guideline 476.[85,86] Briefly, V79-4 cells were seeded on 6-well plates (1 × 10^5 cells per well) and incubated at 37°C and 5% CO_2, 24 h before exposure, The day of exposure, cells were exposed to rGOT at concentrations of (0.1, 10, and 15 μg/mL) for 24 h. At end of exposure the cells were washed, trypsinized, and resuspended in 2 mL medium. The cells were seeded back in ϕ100 mm Petri dishes (3 × 10^5 cells/dish, 3 dishes per sample to achieve approximately 10^6 cells per sample) and grown in complete culture medium for an additional 8 days. Next, the cells were harvested at days 6 and 8 in a selective medium containing 6-thioguanine (6-TG) (5 μg/mL, Sigma). These cells were incubated for another 10 days to allow formation of mutant colonies (6-thioguanine-resistant). At the end of the incubation time, the mutant colonies were stained with 1% methylene blue and counted manually. Only colonies with a minimum of 50 cells were counted. As a positive control Methylmethane sufonate (MMS) (0.1 mM; 3 h) was used. Mutant frequency is expressed as the number of mutant cells per million viable cells and was calculated according to the following formula:

$$Mutant\ frenquency = \frac{number\ of\ mutant\ colonies}{number\ of\ colonies\ from\ untreated\ cells} \times 100$$

Immunohistochemistry

To detect DNA double-strand break, γ-H2AX immunohistochemistry was performed in various cell lines. Basically, half a million cells were grown on coverslips in 12-well plate format. After exposure to 30 μg/mL rGOT and positive control 20 μM etoposide for 24 h, cells were fixed with 4% paraformaldehyde for 15 min at RT and, permeabilized with 0.2% Triton X- for 5 min, and incubated with 1% BSA (in PBS) for 30 min. Next, cells were incubated with γ-H2AX primary antibody (cell signaling; catalog number 9718) diluted in PBS containing 2% BSA (1: 800 dilution) for 24 h at 4°C, and secondary antibody Alexa Fluor 488 anti-rabbit immunoglobulins (Life Technologies). This method was adopted and modified from.[87] After incubation, the coverslips were mounted with 1 μg/mL DAPI and imaged with Zeiss LSM 700 confocal microscope. Minimum 10 images were taken per treatment. The quantification of γ-H2AX immunofluorescence intensity was performed using ZEN blue software (v. 2.3) (ZEISS AG, Oberkochen, Germany) in at least 30–50 cells in two independent experiments.

Chemicals and antibodies

The AlamrBlue kit was purchased from Invitrogen. The Glutamate-Glo assay kit was from Promega. Chlorpromazine hydrocholoride, Methyl methanesulfonate, Cytochalasin B, 6-thioguanine, and Etoposide, were purchased from Sigma. The formamidopyrimidine [fapy]-DNA glycosylase (FpG) enzyme was purchased from New England Biolabs. Glutamate was purchased from Merck. The antibody to detect γ-H2AX was purchased from Cell signaling and the secondary antibody Alexa Fluor 488 anti-rabbit immunoglobulins was purchased from Life Technologies.

Cell uptake analysis of rGOT

Cell uptake analysis of rGOT was developed primary neuronal and astrocytes cultures by labeling the enzyme treatment with rhodamine B isothiocyanate (RITC). Primary neuronal cultures were performed as previous protocol.[88] In brief, C57BL/6J mouse embryo (E15) cortices were isolated, sectioned and then incubated with 0.02% trypsin (Gibco-Invitrogen, Germany). Neurons were seeded at 2 × 105 cells/cm2 in complete Neurobasal medium (Gibco-Invitrogen, Germany), supplemented with 2% B-27 (Gibco-Invitrogen, Germany), 2 mM glutamine (Gibco-Invitrogen, Germany) and 1% PS (Gibco-Invitrogen, Germany) in plates pre-treated with poly-D-lysine (Sigma-Aldrich, Germany), and incubated at 37°C in a humidified 5% CO2-containing atmosphere, for a maturation period of 8–9 days. The purity of neuronal primary cultures was determined using flow cytometry and immunofluorescence analysis. For flow cytometry analysis, neurons were harvested by trypsinization, washed, and resuspended in phosphate buffered saline (PBS). The cells were then fixed and permeabilized using the Cell Fixation and Permeabilization Kit (BD Biosciences, Denmark) and it was stained with Neuron-specific beta-III tubulin APC-conjugated antibody (IC1195A, R&D Systems, Minneapolis, USA) at concentration 1μL/104 cells. After immunostaining, the cells were washed and suspended in 200 μL PBS for subsequent analysis. Analysis was performed using a BD FACSAria II analyzer (BD Biosciences, Denmark). Unlabeled MSCs were used as negative controls. Dead cells and debris were excluded based on side and forward scatter profiles (SSC and FSC, respectively). Staining of negative populations were used to establish compensation parameters. Data were analyzed using the FACSDiva software (BD Biosciences). For immunofluorescence staining, neurons were grown on glass coverslipstreated with 0.1 mg/mL poly-D-lysine hydrobromide (Sigma-Aldrich, Germany). Cells were rinsed with PBS fixed in 4% (w/v) paraformaldehyde (PFA) solution (Thermo Fisher Scientific, Germany) for 10 min at room temperature (RT), and then washed with PBS. Cell permeabilization was performed using 0.25% Triton X-100 (Sigma-Aldrich). Non-specific binding sites were blocked with 0.5% (w/v) bovine serum albumin (BSA) (GE Healthcare, Germany) solution for 30 min at RT. Neurons were incubated with anti-MAP2 antibody (Invitrogen, Netherlands) diluted 1:100 in PBS supplemented with 0.25% Triton X-100 and 15% horse serum for 24 h at 4°C. Cells were washed thrice with PBS and incubated with a biotinylated horse anti-mouse DyLight 549 (Vector Laboratories, California, USA) diluted 1:500 in PBS containing 0.25% Triton X-100 for 2 h at RT. Finally, the cell nuclei were stained with Hoechst stain (Invitrogen, Netherlands) at a concentration of 1:6000 in PBS for 10 min. Cell preparations were mounted with Aqua-Poly/Mount (Polysciences, Germany) and photographed using a Leica (Wetzlar, Germany) DMI6000B with software Leica Application Suite Advance Fluorescence software, version 1.0.0 (Leica Microsystems, Germany). Each *in vitro* assays were performed in triplicate in three independent experiments.

Primary cerebral cortical astrocyte cultures were prepared from postnatal days 1–3 C57BL/6J mice (Charles River, Wilmington, MA, United States) as previously described.[89] Briefly, cortices freed of meninges were incubated in 0.05% trypsin/EDTA (Thermo Fisher Scientific) for 30 min at 37°C, mechanically dissociated, and plated in Falcon Primaria 24-well plates (Becton Dickinson, Lincoln, IL, United States) at 1–2 hemispheres per plate, in Eagle's minimal essential medium, high glucose (Glutamic, Thermo Fisher Scientific) supplemented with 10% fetal bovine serum, (Hyclone, Logan, UT, United States), 100 u/ml penicillin, 100 μg/ml streptomycin (Thermo Fisher Scientific). Cultures were maintained at 37°C in 5% CO2, and medium was changed every 2 days before cell confluence, then twice/week after confluence, and utilized at day *in vitro* (DIV) 21. Cortices collected in ice-cold Eagle's minimal essential medium (Thermo Fisher Scientific) were digested with 0.05% trypsin/EDTA for 15 min at 37°C, triturated, then plated in medium containing 5% FBS and 5% ES (Hyclone). The culture medium was replaced with glial-conditioned medium containing 5% ES and 2% B-27 (Thermo Fisher Scientific). Cytosine arabinoside (3 mol/L, Sigma) was added 24 h after plating to inhibit glial proliferation.

rGOT was labeled with Rhodamine B isothiocyanate (RITC) by mixing 25 RITC/GOT (mol/mol) in in 0.1 M carbonate/bicarbonate buffer. The reaction was left overnight at 4°C and then purified from the excess of RITC by size exclusion chromatography using a PD-10 desalting column. Then, the fluorescently labeled GOT was recovered in the second fraction collected from the PD-10 column. Bradford assay (Pierce TM Coomassie Plus Assay Kit; ThermoFisher #23236) was used to quantify RITC-labelled GOT concentration. Confocal images of fixed cells were captured on an Andor Dragonfly spinning disk confocal system mounted on a Nikon TiE microscope equipped with a Zyla 4.2 PLUS camera (Andor, Oxford Instruments). All the images were processed with ImageJ. Fluorescence intensity from confocal microscopy images was quantified by calculating the corrected total cell fluorescence (CTCF) with ImageJ software.

Characterization of autophagy in HT22 and SH-SY5Y cells and rGOT interaction

HT22 and SH-SY5Y cells were cultured in full DMEM medium, which is DMEM (Sigma-D5671) supplemented with 10% (v/v) fetal bovine serum (FBS), L-glutamine and 100 U/mL penicillin/streptomycin, at 37°C in a humidified 5% CO_2 incubator. Cells were incubated in 1% O_2 condition in New Brunswick Galaxy 48R incubator for 5h to establish hypoxia (H). DMEM with low glucose (1 g/L) without L-Glutamine and without phenol red was used as a hypoxia media. Reoxygenation (R) was conducted following removing cells from hypoxia. Hypoxia media was removed, and media replenished with regular DMEM. Cells were kept under at 37°C in a humidified 5% CO_2, 16.9% O_2 incubator for 5h to establish reoxygenation (H/R).

To detect autophagic flux by quantifying autolysosomes, both HT22 and SH-SY5Y cells were either subjected to hypoxia (H, 5h), hypoxia/Reoxygenation (H/R, 5h) or kept under normal culture condition with or without addition of rGOT (10 μg/mL). Cells were then fixed with 4% paraformaldehyde (Sigma-Aldrich, 15,812-7) and permeabilized in PBS with 0.1% BSA (Sigma, A4503) and 0.1% saponin (Sigma, 84510). Immunostaining was performed using anti-LC3 (Sigma, L7543) antibodies, followed by incubation with anti-rabbit IgG Alexa Flour 488 (Invitrogen, 982425) antibody. Cells also were co-stained with Hoechst (Invitrogen, 33342) for 10 min. Cover slides were mounted and inspected under 63× magnification using a Carl Zeiss LSM 710 confocal microscope (Zeiss, Germany). We previously described the technique in detail in our previous article.[90] Basal autophagy threshold was determined as 5 LC3 puncta per control, non-treated SH-SY5Y and 10 puncta per

control, non-treated HT-22 cells. Puncta in at least 150 cells per experimental point were counted and analyzed. Graphs were plotted as percentage of LC3 puncta positive cells over total cell numbers. Ordinary one-way ANOVA and Student's t test statistical analyses were performed using GraphPad Prism (v.8.3.0) software.

To develop immunoblot analysis, Protein extraction was performed with RIPA buffer (50 mM TRIS-HCl pH 7.4, 150 mM NaCl, 1% NP40, 0.25% Na-deoxycholate) supplemented with complete protease inhibitor cocktail (Roche, 04-693-131-001) and 1 mM phenylmethylsulfonyl fluoride (PMSF; Sigma-Aldrich, P7626). For phosphorylated proteins, protein extraction was performed with RIPA buffer supplemented with complete protease inhibitor cocktail and phenylmethylsulfonyl fluoride (PMSF; Sigma-Aldrich, P7626) and 100 nM okadaic acid, 1 μM cyclosporine A, 1 mM NaF, 50 mM β-glycerophosphate. Cell extracts (30 μg for LC3 shift analysis; 100 μg for the phosphorylation of PERK, eIF2α, and total level of PERK, eIF2α and HIF1α analyses) were separated by SDS-polyacrylamide gels and transferred to nitrocellulose membrane. Following blockage in 5% nonfat milk (or 3% BSA for phosphorylated-protein analysis), membranes were incubated in 3% BSA-PBST solutions containing primary antibodies (ab): anti-LC3B ab (CST, #2775, 1:1000), anti HIF1α ab (CST, #14179, 1:1000) anti-PERK (CST, #3192, 1:1000), anti-p-PERK (Thr 980) (CST, #3179, 1:1000), anti-eIF2α ab (Santa Cruz, sc-133227, 1:1000), anti-p-eIF2α (Ser 51) ab (CST, #3597,1:1000), and anti β-actin ab (Sigma-Aldrich, A5441, 1:10000). Then, the appropriate secondary mouse or rabbit antibodies coupled to horseradish peroxidase (anti-mouse: Jackson Immunoresearch Laboratories, 115035003; anti-rabbit: Jackson Immunoresearch laboratories, 111035144, 1:10000) were applied and protein bands were revealed with chemiluminescence. The band signals were quantified using ImageJ.

To perform qRT-PCR analysis, total RNA was extracted using TRIzol reagent (Sigma-Aldrich, T9424) according to the manufacturer's instructions. cDNA was reverse transcribed from total RNA (DNase treated) using M-MuLV reverse transcriptase (Fermentas, EP0351) or RevertAid enzyme (ThermoScientific, EP0441) and random hexamers (Invitrogen, 48190-011). SYBR Green Quantitative RT-PCR kit (Roche, 04-913-914-001) and a Roche Light Cycler 480 were used for single step qRT-PCR reactions. To activate the SYBR green, an initial cycle of 95°C, 10 min was performed followed by, PCR reactions: 40 cycles of 95°C for 15 s and 60°C for 1 min. Then a thermal denaturation protocol was used to generate the dissociation curves for the verification of amplification specificity (a single cycle of 95°C for 60 s 55°C for 60 s and 80 cycles of 55°C for 10 s). Changes in mRNA levels were quantified using the 2-ΔΔCT method using GAPDH (Gyceraldehyde-3- phosphate dehydrogenase) mRNA as control.

QUANTIFICATION AND STATISTICAL ANALYSIS

All data are expressed as mean ± standard error of the mean. The data were analyzed using SPSS statistical software (v19.0) and GraphPad Prism software (v.8.3.0) for representation of graphs. BioRender (https://biorender.com/) was used for creating the figures. The criterion for statistical significance was set at $p < 0.05$. The Shapiro–Wilk test was used to determine whether the data were normally distributed. Based on the results of normality tests and the sample size, statistical analysis was performed using non-parametric tests, Wilcoxon test for paired data, and Mann−Whitney test for unpaired data.

All data collection and analyses were performed by experimenters who were blinded to the animal's identity and experimental conditions. The exact "n" in each group is specified in the figures. Sample sizes were based on the variance of data in pilot experiments and were generally estimated by power calculations that determined the number of animals required for 80% power to detect a 20–30% difference between groups.